A THEORY OF POLAR SUBSTORMS

by

GERALD ATKINSON

B.A.Sc., University of British Columbia, 1960
M.Sc., University of British Columbia, 1964

A THESIS SUBMITTED IN PARTIAL FULFILMENT OF
THE REQUIREMENTS FOR THE DEGREE OF
DOCTOR OF PHILOSOPHY

in the Department
of
GEOPHYSICS

We accept this thesis as conforming to the
required standard

THE UNIVERSITY OF BRITISH COLUMBIA
AUGUST 1966

In presenting this thesis in partial fulfilment of the requirements for an advanced degree at the University of British Columbia, I agree that the Library shall make it freely available for reference and study. I further agree that permission for extensive copying of this thesis for scholarly purposes may be granted by the Head of my Department or by his representatives. It is understood that copying or publication of this thesis for financial gain shall not be allowed without my written permission.

Department of Geographies

The University of British Columbia
Vancouver 8, Canada

Date Nov. 18, 1966

ABSTRACT

The magnetosphere may be considered as consisting of two regions, the tail and the region of closed lines of force. The interchange of field lines between these two regions is important in magnetospheric processes. Transport of magnetic field lines from the closed region into the tail may occur by Dungey's mechanism or by viscous interaction of the magnetosphere with the solar wind. Transport from the tail to the closed region occurs by recombination through the neutral sheet. Convective flow within the closed region is controlled by the "foot dragging" effect which arises from the discharging action of the ionosphere on flux tubes.

The model of polar substorms presented is a flow or time sequence as follows:

(1) Field lines are dragged from the closed region into the tail by the solar wind, with a resulting storage of potential energy in the tail.

(2) The polar substorm begins when the field lines recombine in an implosive fashion at the neutral sheet, releasing the stored potential energy.

(3) The recombined flux tubes are added to the nightside of the closed region as a giant bulge.

(4) The bulge drives a return flow of flux tubes towardsthe dayside in the closed region.

It is likely that recombination is initiated by the formation of a neutral point at about 13 or 14 earth radii in the antisolar direction, and occurs across a width of tail of about 6 or 7 earth radii, and that 10^8 webers are annihilated in a time of about 1/2 hour. The recombination is probably stopped by the build-up of a giant bulge on the nightside of the closed region, which maps to the earth's surface along field lines as the auroral break-up bulge, and which, as it spreads out over the nightside of the region of closed field lines, causes the observed auroral effects.

The Pedersen current is not expected to produce significant magnetic effects at the surface of the earth except at anomalies in ionospheric conductivity. Such an anomaly along the auroral arcs can explain the westward electrojet. However, it seems probable that the remainder of the polar cap current system is the result of Hall currents.

TABLE OF CONTENTS

FIGURES

TABLE

ACKNOWLEDGMENT

I am deeply indebted to Dr. T. Watanabe both for his patient supervision, and for his many hours of discussion of the ideas expressed in this thesis. I would also like to thank Professor J. A. Jacobs for his encouragement during the preparation of this work, and for his guidance in its final formulation.

This work was supported by the Office of Naval Research under contract Nonr 3116(00).

CHAPTER I

THE MORPHOLOGY OF POLAR SUBSTORMS

Polar substorm is a term used to describe several observed geomagnetic and aeronomical phenomena which occur simultaneously, and are therefore assumed to result from a common cause. Each facet of the polar substorm is discussed in turn below.

a. Auroral break-up (auroral substorm)

The morphology of the auroral substorm has been discussed by Akasofu (1964). He presented it as a time sequence, the essentials of which will be reviewed here. The development is shown in Fig. 1 (for the northern hemisphere).

The quiet phase (T = 0)

When the auroras in the polar region are free from activity for a few hours, those near midnight tend to take the form of quiet homogeneous arcs, lying along geomagnetic latitude circles around 60° - 65°.

The expansive phase

(1) T = 0 - 5 min

The first indication of the start of an auroral substorm is the sudden brightening of one of the arcs.

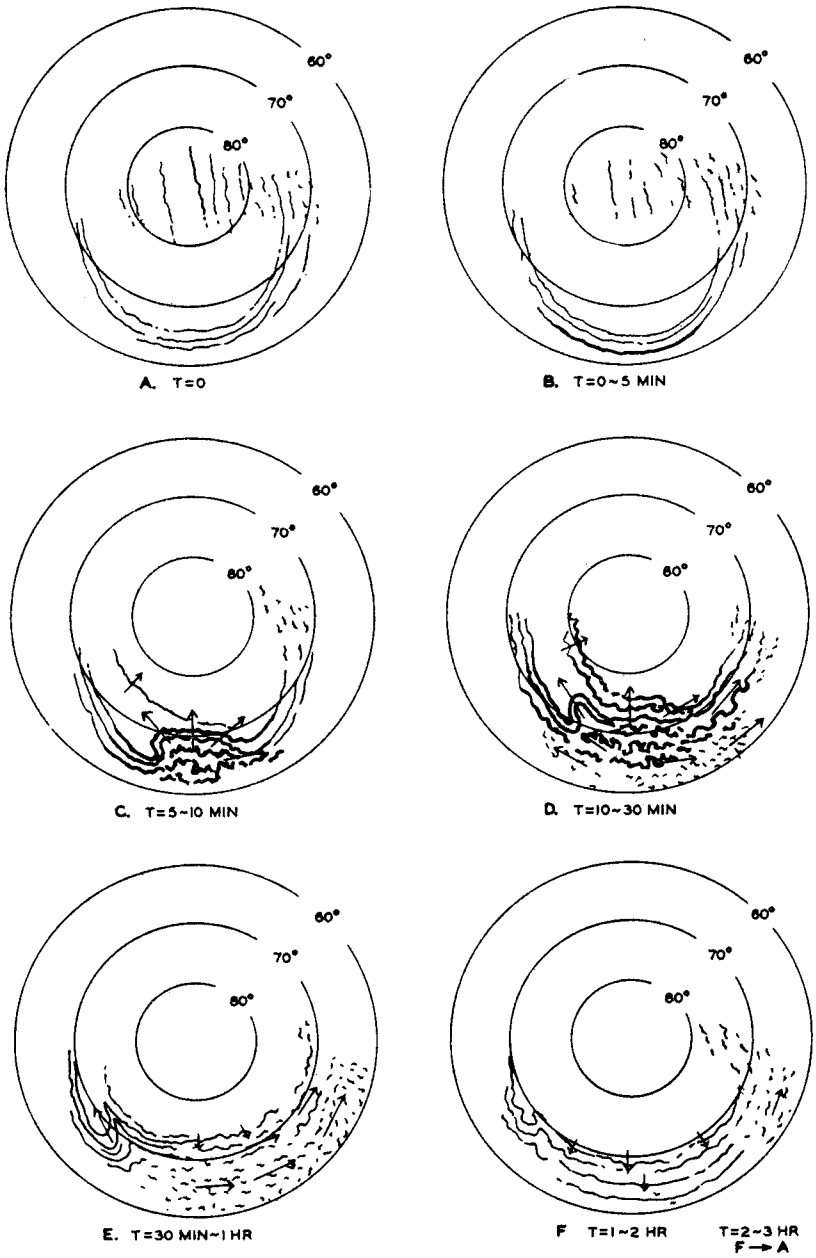

Fig. 1. The time development of the auroral substorm - after Akasofu, 1964. View from above the north pole. Noon is at the top of each diagram.

(2) T = 5 - 10 min

There is a rapid poleward motion of the aurora near midnight, resulting in the formation of a bulge. The bulge tends to expand northward, eastward and westward as shown in Fig. 1. The poleward expansion rate is usually of the order of 20 - 100 km min^{-1}. The bulge is usually centered within an hour of the midnight meridian.

(3) T = 10 - 30 min

During this time, the bands reach their most northerly position (70° - 80° geomagnetic latitude), and those within the bulge are extremely active. Patches appear further south, and all the irregular structure exhibits an eastward drift on the morning side of midnight and a westward drift on the evening side. The western side of the bulge expands rapidly westward at velocities of 10 - 100 km min^{-1}. This feature is called a westward travelling surge.

The intensity of the substorm determines the extent of the northward motion, the amplitude of the surge, and the longitudinal extent over which the disturbances are seen.

The recovery phase

(1) T = 30 min - 1 hr

In this phase, the auroras return southward, usually at speeds less than the poleward motion. The westward surge decreases in velocity and degenerates into small scale

irregular folds or loops. These drift westward at 30 km min^{-1}, and may travel great distances ($\sim$ 1000 km). The brightness of the arcs decreases, and on the morning side the arc structure degenerates into patches which drift eastward at 20 km min^{-1}.

(2) T = 1 - 2 hr

This period is characterized by equatorward motion over a wide range of latitude and longitude and further fading of the arcs.

(3) T = 2 - 3 hr

The slow equatorward motion of faint arcs continues, and no eastward or westward motion of aurora is observed.

b. Geomagnetic bays

The phenomenon known as a negative geomagnetic bay occurs on the nightside of the earth, and is strongest in the auroral zones, where the decrease in the horizontal component of the magnetic field is usually in the range from 100 to 1000 γ . The disturbance is seen with lesser intensity in nearly all latitudes, persisting generally for one or two hours. An example is shown in Fig. 2. The whole magnetic disturbance is called a magnetic substorm (after Chapman - Akasofu, 1964). It is usual to represent the magnetic perturbations by an equivalent ionospheric current system, based on averages over many events. Some of these are shown in

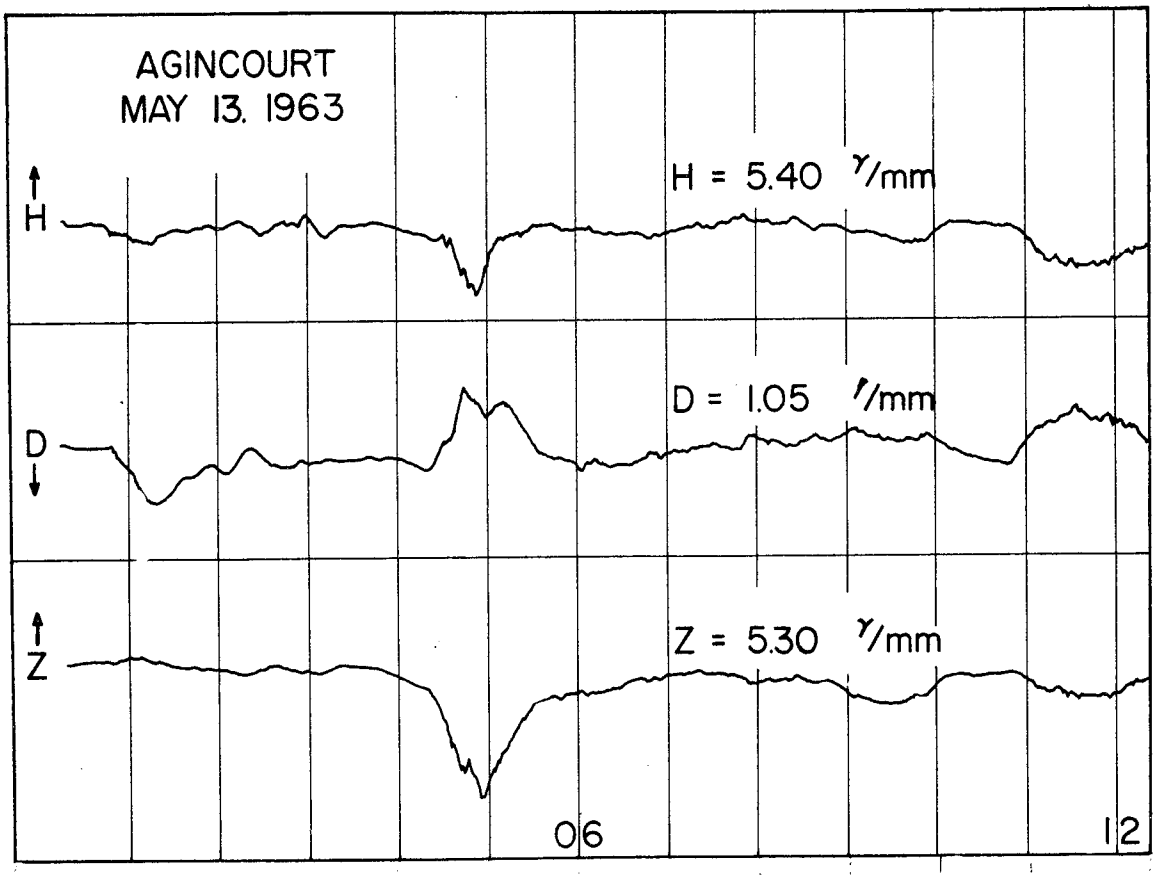

Fig. 2. Example of a negative bay. Agincourt, May 13, 1963.

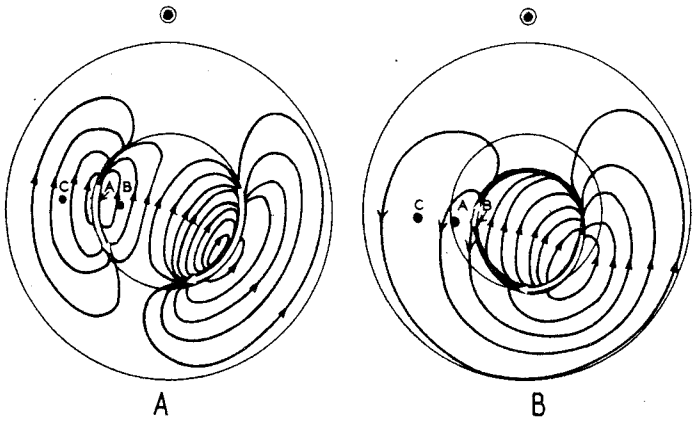

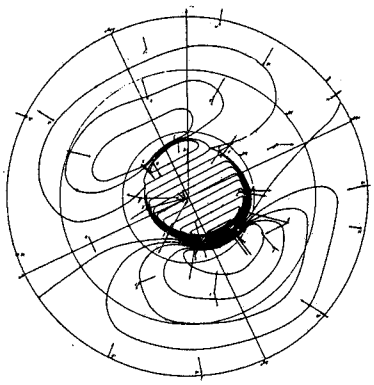

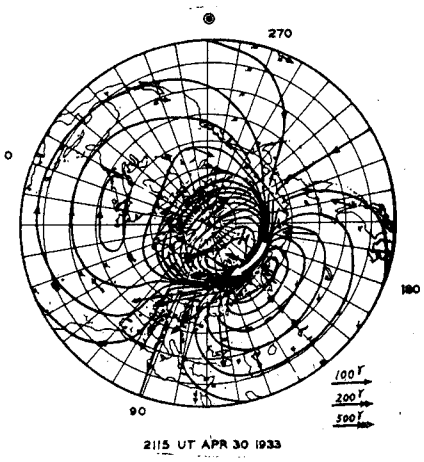

Fig. 3. Bay current systems. (a) Older models.
(b) Model of Akasofu, Chapman and Meng (1965).
(c) Observational results of Vestine.
(d) Observations of Fukushima (1953) of an individual bay.

Fig. 3. Fukushima (1953) suggests that the bay current system is similar to a two dimensional doublet aligned along the auroral zone, and that diagrams such as those in figure 3 are a superposition of many such doublets, reflecting position changes of the basic doublet, rather than the current systems of individual bays.

c. Other phenomena

Other phenomena associated with polar substorms include:

(i) Pi 2 micropulsations. These are irregular pulsations of the geomagnetic field with periods in the range 40 - 150 sec. They coincide with the onset of a geomagnetic bay, and are a nightside phenomenon.

(ii) X-ray bursts. X-ray bursts are observed at balloon altitudes under active aurora. They are believed to be due to electrons ($E \geqslant 25$ kev) bombarding the atmosphere.

d. Satellite observations

(i) O'Brien and Taylor (1964), in an experiment on Injun 3 satellite at an altitude of 950 km, reported an increase in the number of mirroring electrons when the flux of precipitating electrons increased ($E \geqslant 40$ kev). This implies an injection of particles into the magnetic flux tube at times of active aurora.

(ii) Davis (1966) reported large jumps in the proton density ($E \geq 100$ kev) on the nightside of the earth in the trapping region, simultaneous with the observation of geomagnetic bays.

(iii) Heppner (1966), using the EGO results, observed a drop in the magnetic field strength in the tail of the magnetosphere about 15 min after the bay commencement at ground stations. These results are shown in Fig. 4.

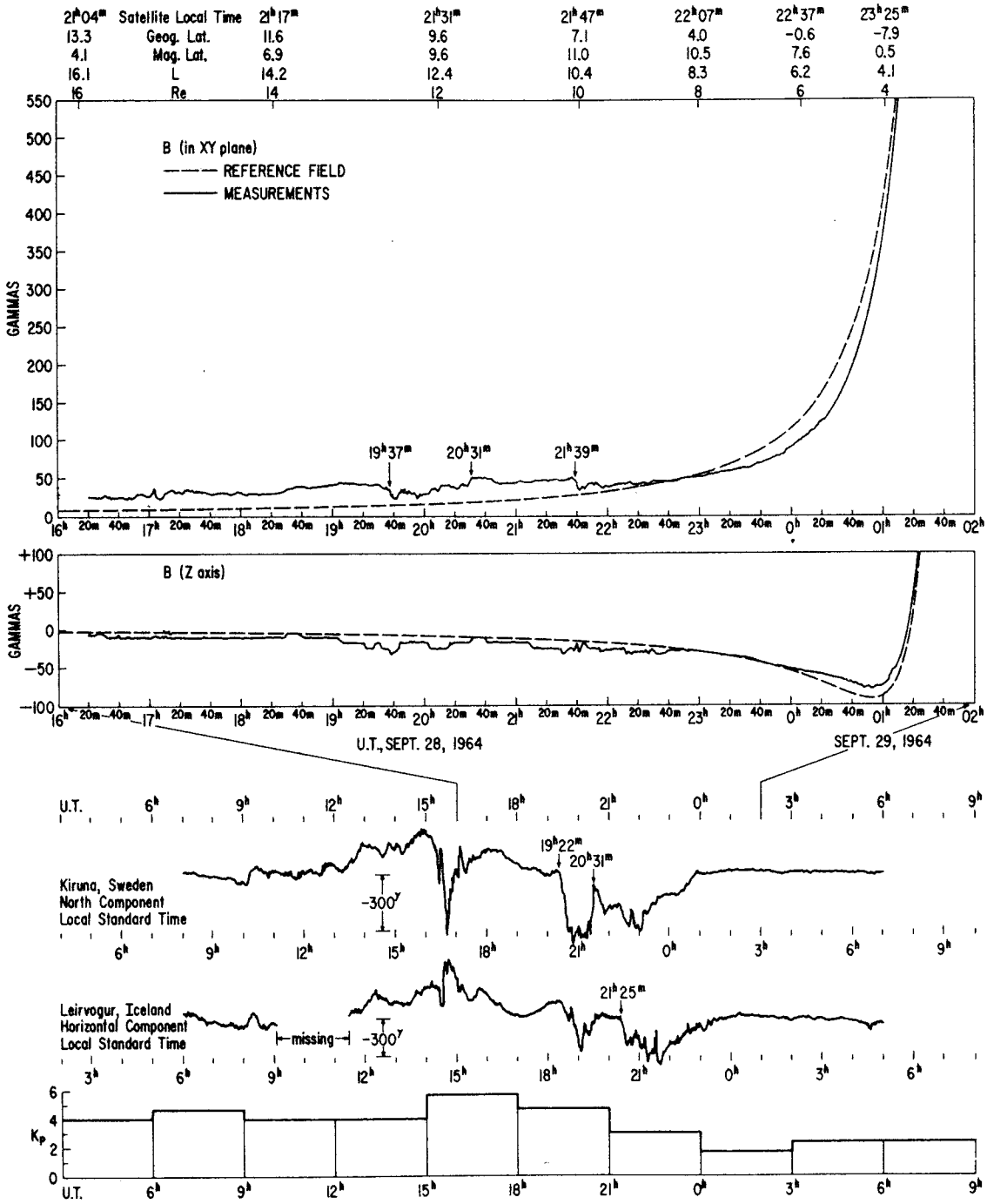

Fig. 4. EGO magnetic field measurements, Sept. 28-29, 1964 - after Heppner (1966), showing decreases in the tail field strength during a geomagnetic bay.

CHAPTER II

THE MAGNETOSPHERE

a. The steady-state magnetosphere

In the open tailed model of the magnetosphere, as defined by Piddington (1960), Axford, Petschek and Siscoe (1965), and Ness (1965), two main regions of space may be defined.

(i) The region consisting of closed lines of force. (See Fig. 5b.) This region is doughnut-shaped with the earth in the central hole of the doughnut. It will henceforth be referred to as the closed region of the magnetosphere, or, for brevity, as the closed region. The rotation of the earth causes the doughnut to rotate about the axis AA in Fig. 5b.

(ii) The region consisting of lines of force not closed in the vicinity of the earth. (See Fig. 5c.) This is commonly referred to as the tail of the magnetosphere, or the tail for brevity. It may be visualized as two "sausages", linked together at the earth, through the hole of the doughnut-shaped region. The force of the solar wind bends these "sausages" in the anti-solar direction so that they wrap around the doughnut in the surface CB of Fig. 5 and are flattened against each other in the plane AB.

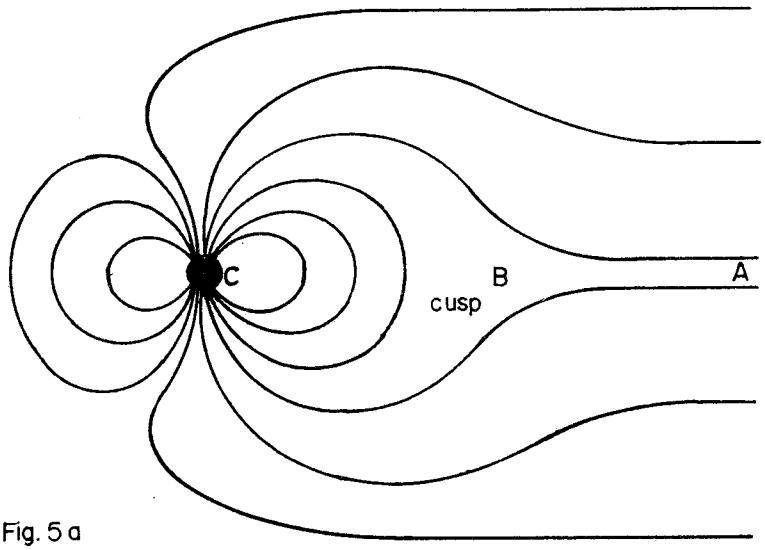

Fig. 5 a

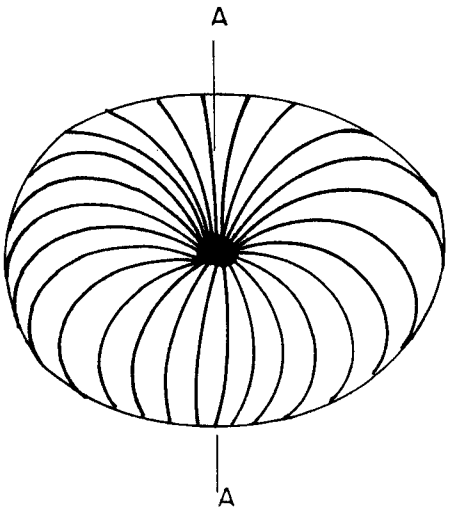

Fig. 5 b

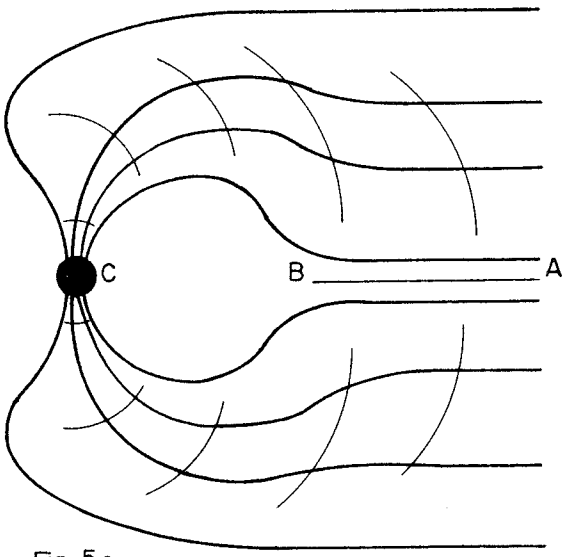

Fig. 5 c

Fig. 5. The open tailed model of the magnetosphere-schematic. (a) Section through the 1200-2400 LT meridian. (b) The doughnut-shaped region of closed field lines. (c) The tail, or region of open field lines.

The rotation of the earth tends to cause these two "sausages" to rotate in opposite directions about their own axes.

b. Interchange of field lines between the regions

There are two mechanisms by which lines of force may move from the closed region into the tail.

(i) Dungey's mechanism. It has been suggested by Dungey (1958) that an oppositely aligned interplanetary magnetic field line can combine with field lines in the closed region of the magnetosphere at a neutral point, and drag it into the tail region. This process is illustrated in Fig. 6a.

(ii) Closed tubes of force may be distended, and dragged by the solar wind from the front and sides of the closed region into the tail. This must occur by friction or viscous like interactions between the solar wind and the magnetosphere. The frictional force could be of many kinds, including wave transmission across the boundary, particle diffusion across the boundary, or instabilities similar to Rayleigh-Taylor, or Kelvin-Helmholtz instabilities which may grow to the extent that flux tubes originally belonging to the closed region could become caught up in the solar wind, and swept into the tail. This is illustrated in Fig. 6b. The frictional processes and instability growth have been reviewed by Piddington (1964).

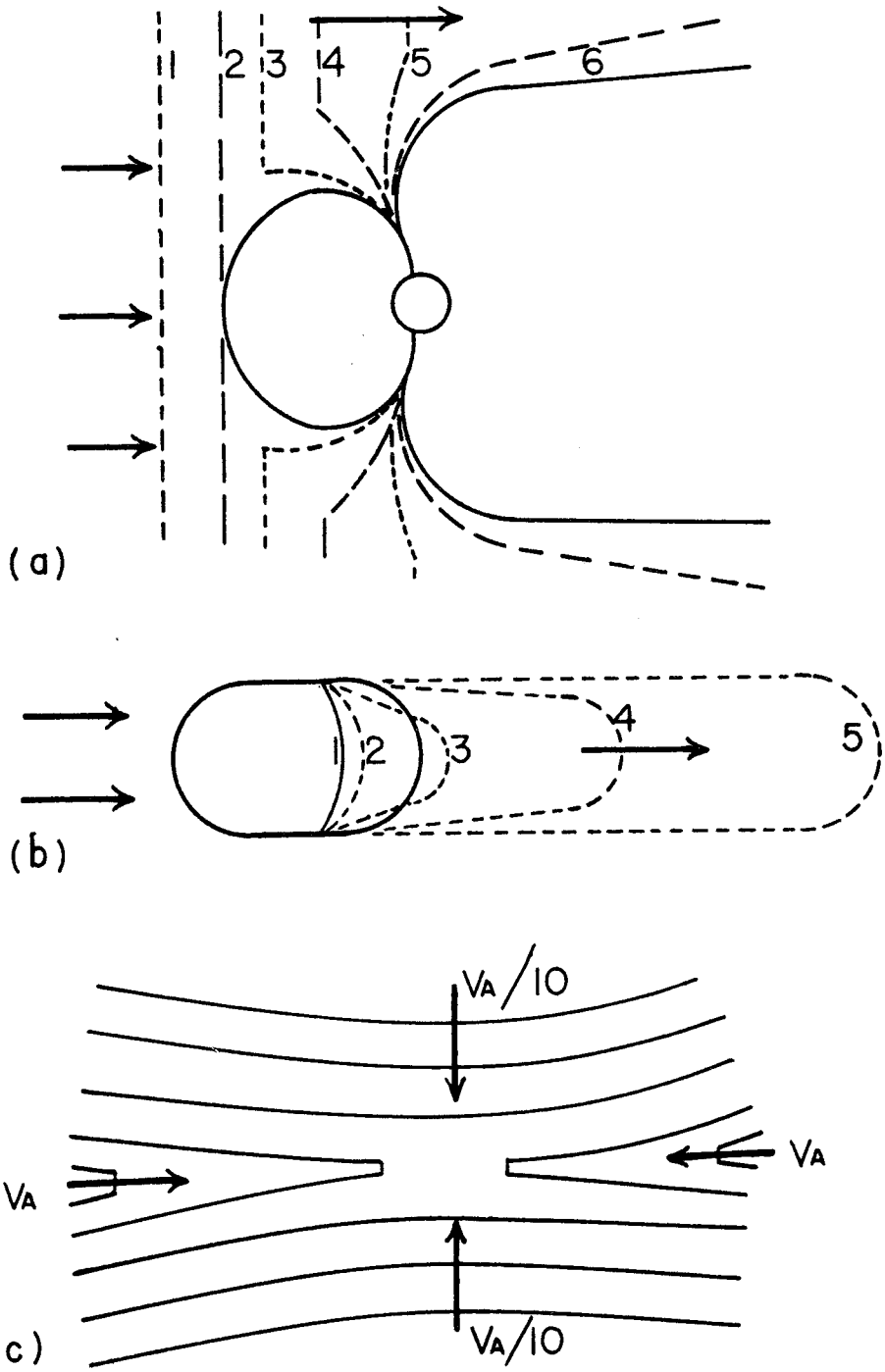

Fig. 6. Interchange of field lines between the regions. (a) Dungey's mechanism - the numbered lines represent successive positions of a field line. (b) Viscous and frictional forces. Loops of field lines originally in the closed region are extended by the solar wind. (c) Sweet's mechanism - the arrows are streamlines of the flow.

The return of the field lines from the tail region to the closed region is accomplished by Sweet's mechanism occurring in the plane AB of Fig. 5 (the neutral sheet). Sweet (1958) considered the recombination of oppositely aligned fields through a neutral sheet. Petschek (1964) has modified this process to allow for the effects of hydromagnetic waves in the removal of gas from the neutral sheet. Axford, Petschek and Siscoe (1965) have applied this theory to the tail of the magnetosphere, assuming a steady state recombination, and found that the flow towards the neutral sheet is $\leq$ 1/10 V_A where V_A is the Alfven velocity in the unperturbed tail. The flow along the neutral sheet towards the closed region is of the order of V_A. The flow patterns are illustrated in Fig. 6c. Magnetic field is annihilated in the neutral sheet, and its energy given to the plasma it contained.

c. Convection within the closed region.

The convection of flux tubes within the magnetosphere has been discussed by Gold (1959). For convective flow to occur, the driving forces for the flow must cause a charge separation, which creates an electric field allowing plasma drift across the magnetic field, as viewed from a stationary reference frame. Because of the high conductivity parallel to the field, field lines are assumed to

be equipotentials, in which case one can speak of the flow of flux tubes, as each tube preserves it identity in such a motion. Viscous forces in the magnetosphere are small, so that convection can occur fairly freely except for the discharging action of the ionosphere on the flux tubes. Gold proposed a model in which there was a sharp transition from frozen field conditions to zero conductivity. In the real case, there should be a drag on the moving field lines due to the Pedersen conductivity of the ionosphere (see Fig. 7). This dissipation was discussed by Axford and Hines (1961). Steady state convection requires that the electric field be maintained. Therefore, there must be a charge separation current produced in the convecting region to offset the discharging action of the ionosphere.

If, in the ionosphere, $\underset{\sim}{E}$ is assumed to be horizontal, and vertically uniform, and $\underset{\sim}{B}$ is assumed to be vertical, then the height integrated discharge current (in the ionosphere) is $\underset{\sim}{J}_i = \sigma_\perp \underset{\sim}{E}$, where $\sigma_\perp$ is the height integrated Pedersen conductivity. Each flux tube experiences a dragging force $\iint (\underset{\sim}{j} \times \underset{\sim}{B})\, dl\, dA = \iint j\, B\, dA\, dl$. For a flux tube $\iint B\, dA$ is constant and $\underset{\sim}{E} = -\underset{\sim}{v} \times \underset{\sim}{B}$. Thus the force on a flux tube of unit area at the ionosphere is

$$B_f \int j\, dl = 2 B_f J_i = 2 \sigma_\perp v_f B_f^2 \text{ newtons} \quad (1)$$

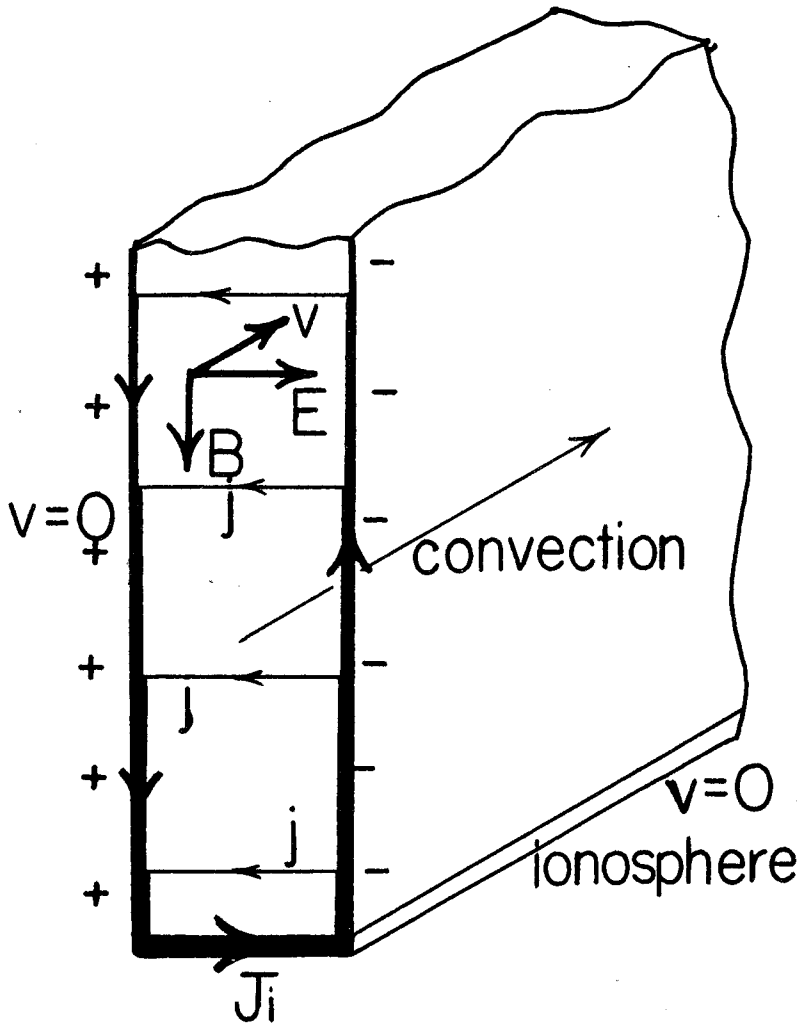

Fig. 7. Cross section of a convecting plasma slab. The plasma convection $\underset{\sim}{v}$, requires the electric field $\underset{\sim}{E} = -\underset{\sim}{v} \times \underset{\sim}{B}$. This causes a discharge current J_i in the ionosphere which must be balanced by a charge separation current j, in the magnetosphere.

where f, used as a subscript, denotes the value at the feet of the field lines. The factor 2 is inserted because each flux tube has two feet.

Consider the Navier Stokes equation integrated over the frozen field region of a flux tube.

$$\int \rho \frac{\partial \underset{\sim}{v}}{\partial t} dV + \int \rho (\underset{\sim}{v} \cdot \nabla) \underset{\sim}{v} \, dV + \int \nabla p \, dV$$

$$- \int (\lambda + \mu) \nabla (\nabla \cdot \underset{\sim}{v}) dV - \int \mu \nabla^2 \underset{\sim}{v} \, dV = \int \underset{\sim}{J} \times \underset{\sim}{B} \, dV \qquad (2)$$

$\underset{\sim}{J}$ is the total current flowing, and includes $\underset{\sim}{j}$, the contribution of the "foot dragging" term. The meaning of the various symbols is given in Appendix I. The order of magnitude of the various terms is considered based on values of the parameters for the magnetosphere given in Table I. In a flux tube B x A is constant, where A is the cross sectional area of the tube. Thus if a mapping factor, g, along flux tubes (equator to feet) is defined by:

$$\begin{aligned} g^2 B &= B_f \quad , \text{ then} \\ A &= g^2 A_f \\ d &\approx g \, d_f \\ gE &\approx E_f \\ v &\approx g \, v_f \end{aligned} \qquad (3)$$

TABLE I

PROPERTIES OF THE MAGNETOSPHERE

	Tail	Magnetosphere (outside knee)	Feet (ionosphere)
Magnetic field (γ)	30	50	50,000
Number density (m^{-3})	2×10^{6}	2×10^{6}	10^{12}
Mass density ($kg\ m^{-3}$)	2×10^{-21}	2×10^{-21}	10^{-15}
Mapping factor -g	41	32	1
Effective length (m)	?	10^{8}	10^{6}
Alfven velocity ($km\ sec^{-1}$)	450	750	1050

where d, E and v denote distances, electric fields and velocities perpendicular to the field lines. In actual fact, the mapping factors for distances measured radially (g_r) and in the angular direction (g_θ) may be different (see Appendix II and Fig. 11). However, the use of $g = \sqrt{g_r\, g_\theta}$ is sufficiently accurate for the purposes of the following calculations.

For a flux tube of unit area in the equatorial plane, the foot dragging term becomes:

$$F = \int \underset{\sim}{j} \times \underset{\sim}{B}\, dV = \int jB\, dV = AB \int j dl$$

but $\int j dl = \frac{2Ji}{g}$

$$\therefore \quad F = \frac{2\,\sigma_\perp V_f\, B_f^{\,2}}{g^3} = 2\ \sigma_\perp\, vB^2 \qquad (4a)$$

Substituting

$$\sigma_\perp = 10 \text{ mho}$$
$$B = 5 \times 10^{-8} \text{ weber m}^{-2}$$

$$F = 5 \times 10^{-14}\ v \quad \text{newton} \qquad (4b)$$

where v is the velocity (m sec^{-1}) of the flux tube in the equatorial plane.

On the assumption that the term on the right hand side of equation (2) contains terms of the size of (4), the energy associated with the various terms can be compared. It is necessary to compare energies, rather than forces, because of the different velocities of different parts of the flux tube. It is for the same reason that (4a) varies from (1) by a factor of g^{-3} rather than g^{-2} as would be expected from area considerations alone. In other words equation (2) should be an equation in angular momentum. In treating it as an equation in linear momentum as is done here, it is necessary to multiply forces at the feet by a "moment arm" of g^{-1}.

The first two terms of equation (2) are of the form $\ell \rho A \frac{dV}{dt}$ representing power $\ell \rho A \frac{V^2}{t}$

Thus the ratio of the contributions near the feet, and in the outer regions of the magnetosphere are:

$$\frac{\ell_f \rho_f A_f V_f^2}{\ell \rho A V^2} = \frac{\ell_f \rho_f}{\ell \rho g^4} \qquad (5)$$

Substitution of values from table I, indicates that the inertial effects of the outer magnetosphere dominate the inertial effects of the feet by a factor of 10^2.

Similarly the power of the fourth and fifth terms of equation (2) is $\sim \ell \mu \frac{V^2}{d^2} A$. The ratio of power near the feet to the outer regions is:

$$\frac{\ell_f A_f \mu_f}{\ell A \mu} = g^2 \frac{\mu_f \ell_f}{\mu \ell} \sim 10^{-5} \mu_f/\mu \qquad (6)$$

It seems unlikely that the ratio $\mu_f/\mu > 10^5$, and the main contribution probably comes from the outer regions.

Thus the assumption is made that the flow is produced by forces in the outer regions of the magnetosphere, and equation (2) is valid if the integrals are restrained to this region. Once this is assumed, it is sufficient to compare forces in equation (2) to determine which terms dominate the flow.

Consider the first term in equation (2). It can be approximated by:

$$F_1 = \ell \rho \frac{v}{t} = 10^{-13} \frac{v}{t} \quad \text{newton} \tag{7}$$

for the values in Table I. Thus this term is not important for flows with a time scale longer than 1 sec, and will have little effect on the large scale flows of the magnetosphere.

Similarly, the second term of equation (2) is of order:

$$F_2 = \ell \rho \frac{v^2}{d} = 10^{-13} \frac{v^2}{d} \quad \text{newton} \tag{8}$$

This term is of the same order as F for

$$\frac{v}{d} \sim 1 \text{ sec}^{-1} \tag{9}$$

This condition is not satisfied for large scale flows in the magnetosphere, and thus F dominates this term. A side result of this is that convective turbulence driven by the main flow should not occur in the magnetosphere.

Consider the fifth term in equation (2). The kinematic viscosity in the outer magnetosphere is probably of the order of 10^9 m^2 sec^{-1} (this is discussed in more detail in Chapter IV). Using the values:

$$\ell \sim 10^{8}\ \mathrm{m}$$

$$\rho \sim 10^{-21}\ \mathrm{kg\ m^{-3}}$$

$$\nu = \frac{\mu}{\rho} \sim 10^{9}\ \mathrm{m^{2}\ sec^{-1}}$$

the fifth term is of order:

$$F_5 = \ell \mu \frac{V}{d^2} \sim 10^{-5} \frac{V}{d^2} \quad \text{newton} \tag{10}$$

comparable with F only when $d < 10^4$ m. This point will be dealt with more specifically in Chapter IV in establishing a boundary layer thickness.

The fourth term or compressibility term is assumed small as $\lambda \sim \mu$. This makes the dimensional analysis the same as the fifth term.

Thus equation (2) can be approximated by:

$$\int \nabla p \, dV = \int \underset{\sim}{J} \times \underset{\sim}{B} \, dV \tag{11}$$

This can be written:

$$\int \left(\frac{\partial p}{\partial x_i} - \frac{\partial \tau_{ij}}{\partial x_j} \right) dV = 0 \tag{12}$$

where τ_{ij} is the Maxwell stress tensor. Thus large scale convective flow within the magnetosphere is controlled by gas pressure and magnetic stresses.

CHAPTER III

THE MODEL OF POLAR SUBSTORMS

The model of polar substorms that the author wishes to present is as follows:

(1) Field lines are dragged from the closed region into the tail by the solar wind, by either or both of the mechanisms already discussed, resulting in an increase of the tail field strength, and a storing of potential energy.

(2) The polar substorm begins when field lines recombine in an implosive fashion at the neutral sheet, in the manner indicated by Petschek (1964). This implies the release of stored potential energy.

(3) The recombined flux tubes are added to the night side of the closed doughnut-shaped region, as a giant bulge, causing the auroral effects.

(4) The flux tubes flow around the closed region towards the dayside causing the magnetic substorm, and further auroral effects.

The above order can be thought of as either a flow sequence or a time sequence. However, it is likely that some of the

stages will be occurring simultaneously. Step (1) is probably a more or less continuous process, depending on the solar wind and interplanetary field conditions. Steps (2), (3), and (4) could and probably do to some extent proceed simultaneously, although step (2) must be initiated before step (3) can occur, and similarly with steps (3) and (4).

Each step will be discussed in turn in the following chapters.

CHAPTER IV

TRANSPORT INTO THE TAIL OF THE MAGNETOSPHERE

The first stage of the model is the dragging of field lines from the closed region into the tail of the magnetosphere by the solar wind. As the field lines are stretched into the tail, potential energy is stored, which can later be released as a polar substorm.

a. Dungey's mechanism

First consider Dungey's mechanism. When the transition region magnetic field is antiparallel to the earth's field, the analysis of Petschek (1964) can be used, and combination occurs at 1/10 V_A (Axford, Petschek and Siscoe, 1965). A field of 20γ and a proton number density of 10^7 m^{-3} is perhaps a reasonable estimate for conditions in the transition region at the subsolar point. (A density jump by a factor of 3 or 4 over interplanetary conditions is expected - Spreiter et al., 1966.) Thus $V_A \approx 140$ km sec^{-1}, and magnetic flux is transported into the tail at a rate of 2×10^4 webers sec^{-1}, assuming that combination occurs across a region 10^8 m wide at the front of the

magnetosphere. It will be shown in later chapters that polar substorms involves the collapse of 10^8 webers from the tail into the nightside of the closed doughnut-shaped region. At the above rate, sufficient field could be transferred to the tail for a substorm in 1 1/2 hours. In active times, substorms occur every few hours (Akasofu, 1964).

The above rate is expected to be an overestimate, and could be out by orders of magnitude. The error arises principally from the assumption of antiparallel fields. In fact, theory predicts (Parker, 1963), and satellite observations confirm (Ness et al., 1965) that the interplanetary field lines lie primarily on the surface of cones of constant solar latitude, or approximately parallel to the solar equatorial plane at the earth's orbit. However, there are many temporal fluctuations, and this mechanism could contribute significantly to the transport of flux tubes into the tail.

b. Viscous forces

Another way in which field lines may be transported into the geomagnetic tail is by viscous-like interaction at the outer boundary of the closed doughnut-shaped region. The rate of transport into the tail should be determined by the viscosity of the medium. Axford (1964) predicted

a kinematic viscosity of 10^9 m^2 sec^{-1} to account for flow patterns within the magnetosphere, and then showed that sound waves crossing the boundary could produce this. Parker (1958) obtained the same figure assuming that the viscosity was produced by the scattering of particles by magnetic field inhomogeneities.

In Chapter II, an order of magnitude calculation indicated that viscosity was important only for flow distance scales $< 10^4$ m. A more exact boundary analysis is carried out below.

Consider a flux tube shear flow involving a thin surface layer of the closed region (assumed cylindrically symmetric, and steady-state flow). The flow is in the θ direction, and is driven by a flow outside the boundary. (See Fig. 8a.) Curvature effects are neglected. Equation (2) becomes, for forces in the θ direction:

$$\int \rho \nu \frac{d^2 v_\theta}{d r^2} \, dV = \int \tau_{i\theta} \, n_i \, dS \tag{13}$$

where n is the unit normal vector to the surface. For a tube 1 m by 1 m at the equator, equation (13) can be approximated by:

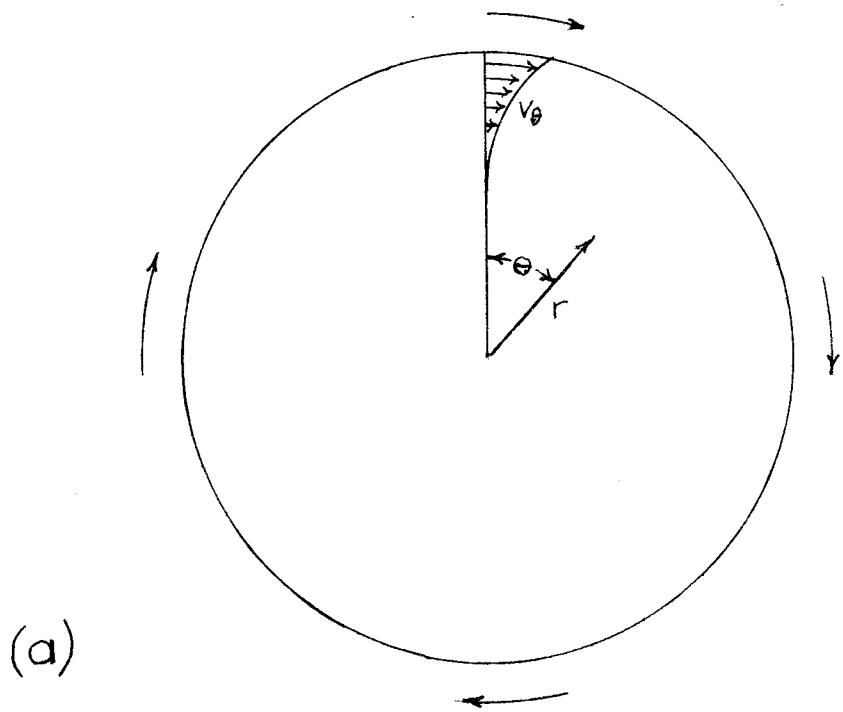

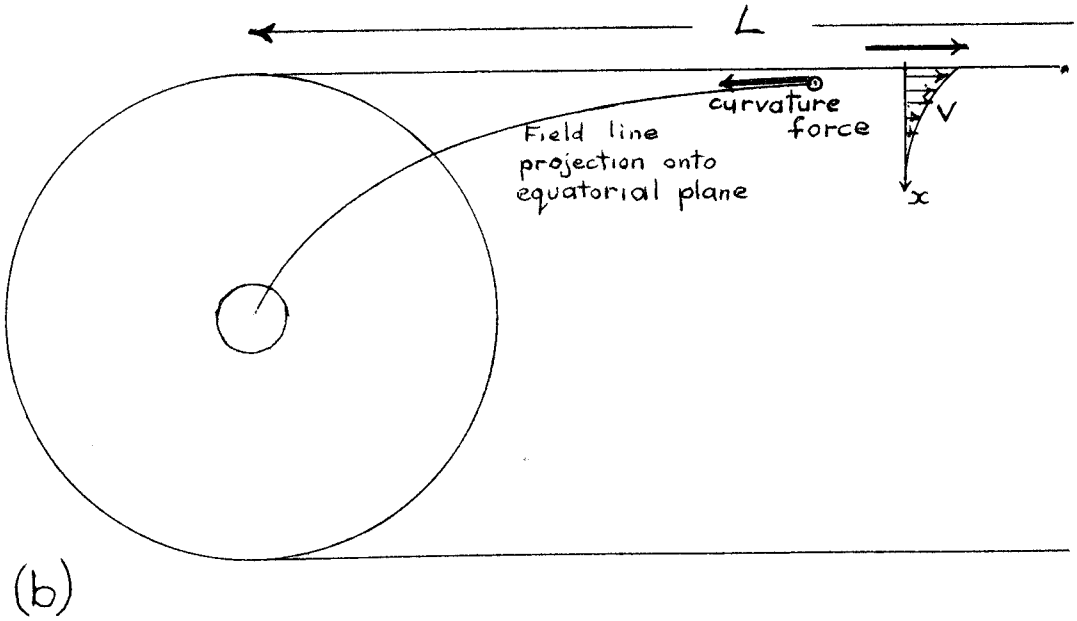

Fig. 8. (a) Shear flow at the boundary of the magnetosphere. Idealized problem.
(b) Shear flow into the tail.

$$\ell \rho \nu \frac{d^2 v_\theta}{d r^2} = \frac{2 \sigma_\perp B_f^2}{g^3} v_{f\theta}$$
$$= \frac{2 \sigma_\perp B_f^2}{g^4} v \qquad (14)$$

The term on the right hand side is the "foot dragging" term, which is the shear stress across the feet of the tubes. Symmetry requires that the Maxwell stresses on the other surfaces cancel. The solution for v is exponential, decreasing with depth to 1/e of its value in a distance

$$\left(\frac{g^4 \rho \nu \ell}{2 \sigma_\perp B_f^2} \right)^{\frac{1}{2}} \approx 5 \times 10^4 \text{ m} \qquad (15)$$

using values of the parameters:

$g = 32$

$n = 10^6 \text{ m}^{-3}$

$\nu = 10^9 \text{ m}^2 \text{ sec}^{-1}$

$\ell = 10^8 \text{ m}$

$\sigma_\perp = 10 \text{ mho}$

$B_f = 50{,}000\ \gamma$

The corresponding rate of flux transport towards the nightside is250 webers sec^{-1}, assuming that $B = 50\gamma$, and that the boundary layer is dragged along at a velocity

of 10^5 m sec^{-1} by the solar wind. This implies a time of 10^6 sec to build up enough energy for a substorm. This is a factor of 10^2 too long, but considering the nature of the calculations, and the uncertainty in ν (the value of which could vary by 2 or more orders of magnitude), this process cannot be ruled out as the mechanism of transport into the tail.

If this mechanism is dominant, the field lines will flow towards the nightside, and then be stretched into the tail. Consider the flow during the stretching process. (See Fig. 8b.) The field lines, due to tension effects, feel a force approximately in the solar direction of magnitude $B^2/\mu_0 R$ where R is their radius of curvature. If the dragging force is viscous, the equation for the flow is:

$$\rho \nu \frac{d^2 v}{d x^2} = \frac{B^2}{\mu_0 R} \tag{16}$$

A solution to this equation is:

$$v = \frac{B^2}{2 \mu_0 R \rho \nu} (x - x_0)^2$$

$$= 2 \times 10^{-6} (x - 2.2 \times 10^5)^2 \text{ m sec}^{-1},$$

using values:

$$B = 30\ \gamma$$
$$\nu = 10^9\ m^2\ sec^{-1}$$
$$n = 10^6\ m^{-3}$$
$$R = 10^8\ m$$

and the boundary condition $v\ (x = 0) = 10^5\ m\ sec^{-1}$. Pressure-like terms in the Maxwell stress tensor give a force of the order $\frac{B^2}{2\mu_0 L}$ (the pressure gradient). As the flow is believed to extend to very large distances in the antisolar direction, $L \gg R$, and these terms can be neglected. This solution falls to 1/e of its value in $.9 \times 10^5$ m. Thus the rate of flow into the tail by viscous mechanisms is probably controlled by the ability of flux tubes to convect around the sides of the magnetosphere, rather than by their stretching into the tail.

CHAPTER V

FIELD LINE RECOMBINATION

The recombination of field lines across a neutral sheet has been discussed by Sweet (1958) and modified by Petschek (1964) for the steady state case. A maximum flow towards the neutral sheet of 1/10 V_A was estimated for the magnetosphere by Axford, Petschek and Siscoe (1965). The flow takes this maximum value when the geometry is as shown in Fig. 6c. However, the flow can be controlled by other factors such as the build up of a back pressure preventing the outflow along the neutral sheet of Fig. 6c, or the hampering of the inflow if the field lines in the plasma flowing towards the neutral sheet develop a greater curvature (i.e. magnetic tension effects restrict the flow). For recombination to proceed impulsively, as required by the model, a triggering and a choking mechanism are needed.

a. Triggering mechanism

The triggering is probably determined by conditions in the neutral sheet which should be influenced by the field strength in the tail - a stronger field producing a greater stress across the neutral sheet. This is probably

the cause of the higher occurrence frequency of substorms during geomagnetic storms, when the tail field strength is higher. Fig. 4 shows a gradual decrease in field strength further back in the tail (except for temporal fluctuation at 1937 and 2139 UT). This is due to the expansion of the tail in the antisolar direction. Fig. 4 shows values of 40 - 50γ around 9 to 13 earth radii, but only 25 - 30γ beyond 14 earth radii. This is consistent with the Imp I results (Ness et al., 1965) which indicate a tail radius increase of 2 or 3 earth radii in going from 10 to 20 earth radii in the antisolar direction.

Similarly there should be a decrease in total field as the cusp is approached, just outside the closed region. The location of the cusp is perhaps best indicated by the Imp I particle experiments. Anderson (1965) places the limit of the stably trapped region at 8 earth radii, and calls a region of plasma extending from 8 to 14 earth radii the cusp. This is presumably plasma temporarily trapped in the region of depressed magnetic field around the cusp.

Thus the tail field probably exerts the maximum stress across the neutral sheet at about 13 or 14 earth radii in the antisolar direction. This is the most likely place for the neutral point of Sweet's mechanism to form,

and for the recombination to be triggered. Once a normal component is established, hydromagnetic forces sweep aside the neutral sheet plasma, and the recombination proceeds implosively. As the geometry is at first similar to that of Petschek (1964), the recombination should occur initially at 1/10 V_A.

b. Choking mechanism

The choking mechanism is probably a hydromagnetic back pressure. It is expected that a large bulge (discussed further in Chapter VI) will build up on the nightside of the earth, and will restrict the flow pattern of Fig. 6c. The bulge is expected to extend several earth radii on the nightside of the closed region, and will move the boundary of the closed region, and the cusp outward by a similar amount. This places the original neutral point well inside the cusp, where recombination is hampered by the curvature of the field lines, and consequent lower stress across the neutral sheet, and perhaps also by the back pressure from the outflowing gas. It is possible that the neutral point moves outward ahead of the cusp. Motion of this type would bring it into a region of weaker field, further in the tail, with a consequent slowing down of the recombination rate. However, for recombination to stop entirely, it seems likely that there must be a gas pressure build up at the neutral point.

c. Energy of recombination

The magnetic field energy that is annihilated in the recombination is given primarily to the particles which it contained. These cause the auroral brightening associated with a substorm. If the tail field strength is 30γ, and a number density of 10^6 m^{-3} is assumed, then from the relationship $\frac{B^2}{2\mu_0} = En$, the energy (E) given to the particles is 4 kev, in reasonable agreement with the particle energies causing visual aurora.

An estimate of the energy flux of auroral electrons is 400 ergs cm^{-2} for a bright aurora (Chamberlain, 1961). If a flux of this order lasts for 10^3 sec (the duration of the auroral substorm expansive phase) on an area 100 km by 1000 km, the total energy is 3×10^{20} ergs. The volume of tail field that must be annihilated to produce this energy has a linear dimension of 4×10^7 m, or 6 1/2 earth radii. This is in good agreement with the length of the tail involved in the recombination predicted earlier in this chapter. (The length will include field from the boundary of the closed region out to the neutral point or region of maximum stress.) If the dimensions of the cross sectional area are the same, and the field is 30γ, this represents a flux of 5×10^7 webers, in close agreement with the value of 10^8 webers assumed herein.

The recombination rate is initially 1/10 V_A, or 45 km sec^{-1} (see Table I). To annihilate 10^8 webers through a slot 4 x 10^7 m wide at this rate takes 30 min, which is the duration of the expansive phase of the auroral substorm (Akasofu, 1964).

CHAPTER VI

BULGE ADDED ON THE NIGHTSIDE OF THE CLOSED REGION

The recombination of field lines at the neutral sheet results in the addition of flux tubes to the nightside of the closed doughnut-shaped region. The inflow into the nightside occurs initially at a rate of V_A, whereas the outflow is much slower because of the foot dragging effect. Thus a large bulge is expected to form, as shown in Fig. 9. The flow pattern during the collapsing phase is shown in Fig. 10.

If the location of the aurora is the map along field lines of the inner edge of the neutral sheet, then the addition of a bulge to the nightside of the closed region should result in a northward bulge of the auroral arcs into the polar cap (southward at the southern pole), as is seen in Fig. 1c. The dimensions of the bulge in Fig. 1c are 1000 km by 1000 km, and the field is 50,000γ, giving a flux of 5×10^7 webers in the bulge, in agreement with the 10^8 webers earlier associated with a substorm. As $g = 32$, this maps as a bulge of 5 earth radii on the nightside of the closed region. It cannot, however, be

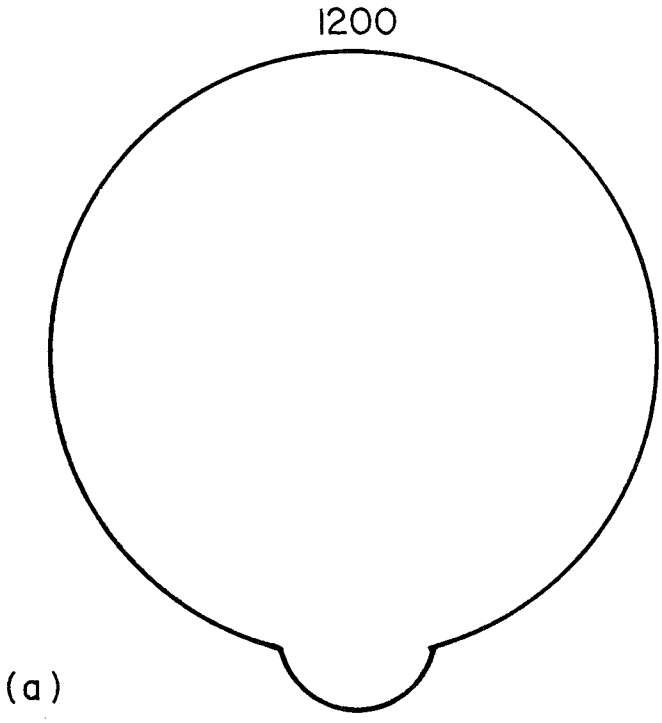

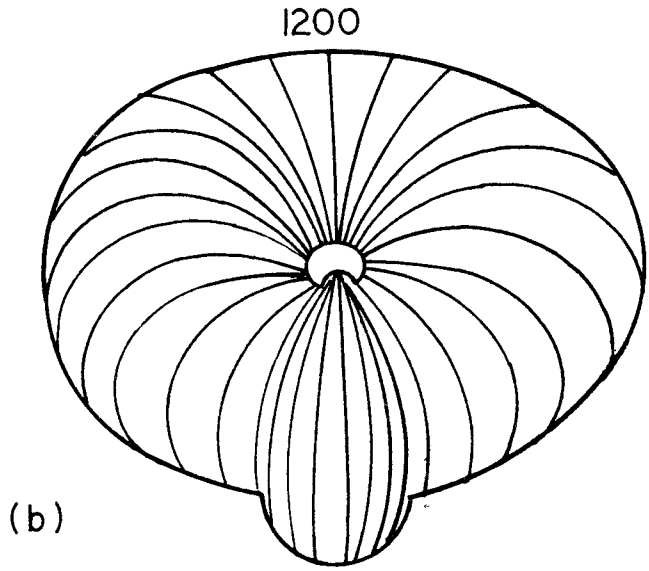

Fig. 9. Bulge on the nightside of the closed region. (a) equatorial section. (b) pictorial view.

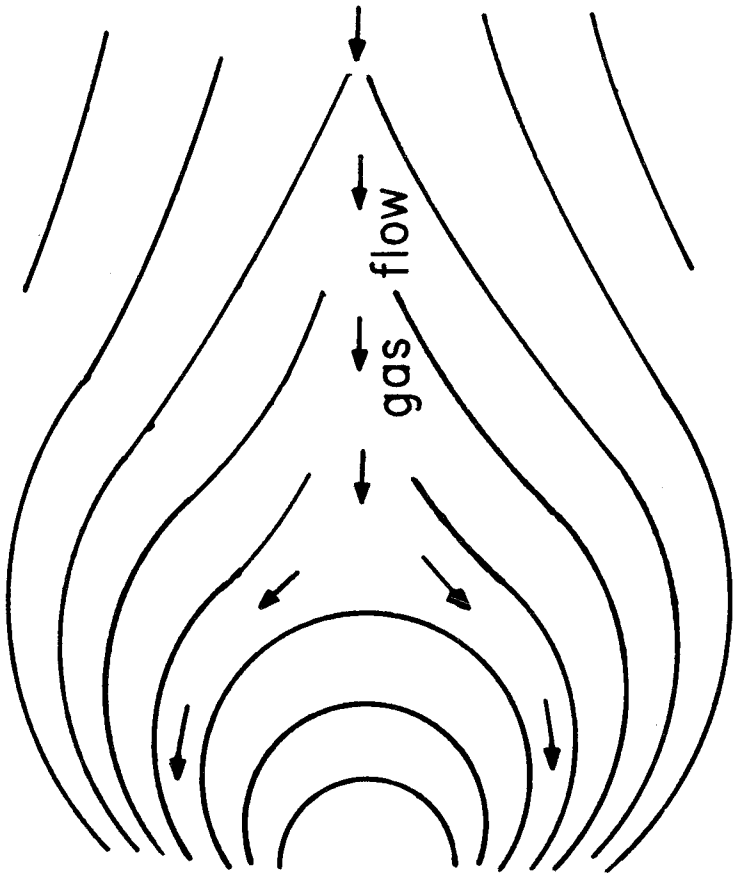

Fig. 10. Flow pattern during the collapsing phase.

assumed that shapes will be exactly preserved in mapping along field lines. This would only be the case if the field lines were constrained to lie in meridian planes. The actual bulge is likely to be somewhat flatter in the equatorial plane, than at the feet, as the flux tubes bend away from a high pressure region. (Hydromagnetic pressure $P = B^2/2\mu_0 + p$.)

The northward expansion rate of Akasofu's bulge can be predicted from the model. Recombination occurs initially at 1/10 V_A (45 km sec^{-1}. See Table I.) This maps as 1 km sec^{-1} in the auroral zone. Akasofu (1964) quotes 0.3×10^3 to 1.7×10^3 m sec^{-1} as being typical observed values. It should be emphasized that this does not involve significant motion of the feet of the field lines, only of the mapping of the inner edge of the neutral sheet, and there is therefore no "foot dragging" effect restricting the northward expansion of the bulge.

The large flux tube added to the nightside contains field lines which have just recombined, and which, therefore, contain energetic plasma. Thus, inside the bulge should be an active auroral region, and this is in fact indicated by Akasofu's diagrams (Fig. 1.). Many auroral patches are observed inside this region.

The Pi 2 type micropulsation activity at this time can be understood in terms of the "closing" flux tubes bombarding the nightside of the magnetosphere at high velocities. Transverse waves are excited and guided into the auroral zones by the field lines.

The observations of Injun III (O'Brien and Taylor, 1964) add support to this picture, in that an increase of the trapped electron flux ($E \geq 40$ kev) is observed on the nightside at times of enhanced auroral activity.

Davis (1966) reported a depletion of energetic protons in the closed region on the nightside at times of a geomagnetic storm. The recovery phase contained a series of polar substorms, and with each substorm there was a sudden step-like increase in the proton count, implying impulsive injection of energetic particles, as would be expected from the model. The measurements were for protons of energy $>$ 100 kev.

At the time of the maximum northward extent of the bulge, the flow into the bulge must equal the flow out. The flow into the bulge is 54,000 webers sec^{-1} (i.e. the recombination rate at the neutral sheet at 45 km sec^{-1}, through a slot 4×10^7 m wide, and a tail field strength of 30γ). An inspection of Fig. 1 shows that the outflow

from the bulge extends over a range of about 15° in latitude, or 1500 km. If the outflow of flux tubes through meridians on each side of midnight is considered, an outflow velocity of 350 m sec^{-1} is predicted, in agreement with observed eastward and westward drift rates. In this calculation, the assumption has been made that the recombination rate has not slowed down at the time of maximum northward extent, and this drift rate should therefore be a maximum value.

CHAPTER VII

RETURN FLOW TO THE DAYSIDE

a. The flow

Once the bulge has been deposited on the nightside of the earth, it may be expected to drive a return flow towards the dayside in the outer regions of the closed doughnut-shaped region. This type of motion appears in Figs. 1 c, d, e, f. The auroral patches and irregular structure are observed to drift eastward on the east side of the midnight meridian, and westward on the west side, indicating outflow from the midnight meridian. The giant bulge is expected to spread out over the surface of the closed region as part of this general flow.

b. An approximate flow equation and solution

When the bulge is first deposited, there should be an immediate deformation of the flux tubes, at Alfven velocities, with negligible foot motion. Further flow must then occur by the dragging of the feet through the ionosphere. This flow should be much slower than the Alfven velocity.

To put this on a mathematical basis, and obtain some idea of the flow, the assumption is made that flux

tubes are confined to lie approximately in meridian planes in their convection within the magnetosphere (i.e. $B_\theta \ll B$), and mirror symmetry exists in the equatorial plane. Thus for flow in the θ direction, equation 12 gives:

$$\int \left(\frac{\partial p}{\partial x_\theta} - \frac{\partial \tau_{\theta j}}{\partial x_j} \right) dV = 0 \tag{18}$$

The coordinate system is shown in Fig. 11. x_θ is used rather than θ to indicate that the system will be treated as Cartesian, curvature effects in the θ direction being ignored. Equation (18) can be integrated over a tube 1m by 1m at the equator to give the approximate relation:

$$\ell \frac{\partial p}{\partial x_\theta} + \ell \frac{\partial}{\partial x_\theta}\left(\frac{B^2}{2\mu_0}\right) + \frac{2\sigma_\perp V_{f\theta} B_f^2}{g^3} = 0 \tag{19a}$$

or

$$\frac{\partial P}{\partial x_\theta} = -\frac{2\sigma_\perp B_f^2}{\ell g^4} V_\theta$$

$$= -A V_\theta \tag{19b}$$

where $$A = \frac{2\sigma_\perp B_f^2}{\ell g^4}$$

and $P = p + B^2/2\mu_0$ is the hydromagnetic pressure. The third term of equation (19a) is the foot dragging

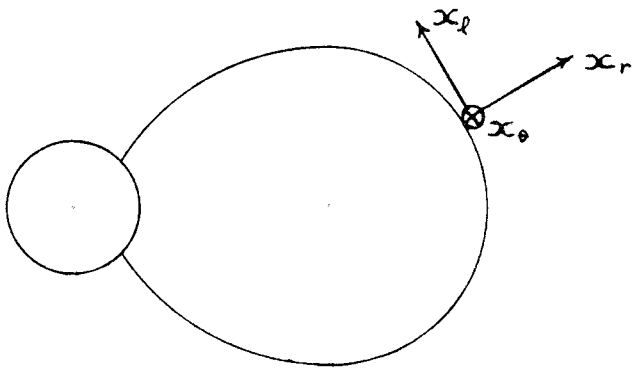

Fig. 11. Coordinate system.

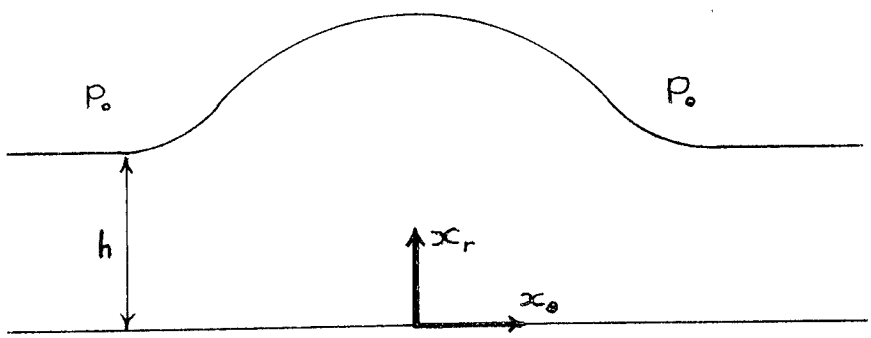

Fig. 12. Geometry for equation (24).

term, and is the Maxwell stress ($\frac{B_\ell B_\theta}{\mu_0}$) in the θ direction on the feet of the tube. It is assumed that the foot dragging term is the only stress on the feet in the θ direction. The other two terms are the gas pressure and Maxwell stress on the sides of the tube.

For those who find the concept of Maxwell stress unsatisfactory, equation (11) can be written:

$$\int \frac{\partial p}{\partial x_i} \, dV = -\int \frac{\partial}{\partial x_i}\left(\frac{B^2}{2\mu_0}\right) dV + \int \frac{B_j}{\mu_0} \frac{\partial B_i}{\partial x_j} \, dV$$

or approximately:

$$\frac{\partial P}{\partial x_\theta} \, \ell A = \frac{A B_\ell}{\mu_0} \int_{f_2}^{f_1} \frac{1}{g_\ell} \frac{\partial B_\theta}{\partial x_\ell} \, d\ell$$

$$= \frac{B_{\ell f}}{\mu_0 g} \left(B_{\theta f_1} - B_{\theta f_2} \right) A_f$$

where f_1 and f_2 denote the two feet of the tube. It is shown in Chapter VIII, equation (32) that

$$B_{\theta f_1} \approx - B_{\theta f 2} \approx \mu_0 \sigma_\perp V_{f\theta} B_f$$

and equation (19) follows.

The error in applying equation (19) to flux tubes not confined to meridian planes, assuming the angular departure is not too large, arises not so much from the fact that they are at an angle to the meridian planes, as from the

further distortion or shape change that such a tube undergoes in the flow (i.e. the greatest error is probably due to changes in the energy of the magnetic field in the flux tube).

A consistent assumption in considering flow in the r direction is that the "foot dragging" term acts as a perturbation on the shape of the flux tube. Then equation (12) can be written:

$$\ell \frac{\partial p}{\partial x_r} + \ell \frac{\partial}{\partial x_r}\left(\frac{B^2}{2\mu_0}\right) + \ell\left(\frac{B^2}{\mu_0 R}\right) + \frac{2\sigma_\perp V_{fr} B_f^2}{g^3} = 0 \tag{20}$$

where R is an appropriate average radius of curvature of the flux tube in the unperturbed state ($\sigma_\perp = 0$). The third term in equation (20) arises from the stress tensor component:

$$\frac{B_\ell}{\mu_0} \frac{\partial B_r}{\partial x_\ell} \approx \frac{B^2}{\mu_0 R} \tag{21}$$

The justification for this is as follows:
If a field line is locally approximated by a circular arc, then it obeys the equation:

$$x^2 + y^2 = R^2$$

in an x, y plane with the origin at the center of curvature.

Then $$\frac{dy}{dx} = -\frac{x}{y} \approx -\frac{x}{R}$$

for small x.

Therefore $$B_y \approx -B\frac{x}{R}$$

$$\frac{dB_y}{dx} = -\frac{B}{R}$$

and equation (21) follows.

A comparison of the third and fourth terms of equation (20) using the following values for the parameters:

$$\begin{aligned} \sigma_\perp &= 10 \text{ mho} \\ \ell &= 10^8 \text{ m} \\ R &= 10^7 \text{ m} \\ B &= 50\ \gamma \\ B_f &= 50{,}000\ \gamma \\ g &= 32 \\ v_{fr} &\sim 10 \text{ m sec}^{-1} \end{aligned} \tag{22}$$

indicates that the third term dominates the fourth by 3 orders of magnitude. An inspection of Fig. 1 shows little northward or southward motion of flux tube feet, i.e. the

auroral drift motions are predominantly eastward or westward. v_{fr} is therefore small, and the approximation:

$$\frac{\partial P}{\partial x_r} = -\frac{B^2}{\mu_0 R} \tag{23}$$

can be used instead of (20). Physically equations (19) and (23) imply that curvature forces in the x_r direction cause pressure gradients, and therefore flow in the x_θ direction, opposed by the foot dragging effect.

A solution to equations (19) and (23) for the geometry of Fig. 12, is:

$$P = P_0 + \left(h(x_\theta) - x_r\right)\frac{B^2}{\mu_0 R} \tag{24}$$

Thus from equation (19):

$$V_\theta = -\frac{1}{A}\frac{B^2}{\mu_0 R}\frac{dh}{dx_\theta}$$

or substituting values in (22):

$$V_\theta = -3\times10^5 \frac{dh}{dx_\theta} \quad m\ sec^{-1} \tag{25}$$

or

$$V_{f\theta} = -10^4 \frac{dh}{dx_\theta} \quad m\ sec^{-1} \tag{26}$$

If it is assumed that figure 1 is a map of the bulge shape, slopes of order 0.1 exist on the morning side, implying foot flow velocities of several hundred m sec^{-1} in agreement with the observed drift velocities of auroral patches (Akasofu, 1964).

An attempt is now made to get a wave equation for the flow. If the fluid is assumed incompressible, the equation of continuity, div v = 0, can be replaced by:

$$-\frac{\partial h}{\partial t} = \frac{\partial (h v_\theta)}{\partial x_\theta} \tag{27}$$

Substituting (25) into this:

$$\frac{\partial h}{\partial t} = \frac{3 \times 10^5}{2} \frac{\partial^2 h^2}{\partial x_\theta^2} \quad m\ sec^{-1} \tag{28}$$

If equation (28) is linearized by writing $h = h_o + h^1$ (h_o constant):

$$\frac{\partial h^1}{\partial t} = 3 \times 10^5 h_o \frac{\partial^2 h^1}{\partial x_\theta^2} \quad m\ sec^{-1} \tag{29}$$

This is the diffusion equation, and the substitution of a small amplitude sinusoid gives a phase velocity of $6 \times 10^{12} k$ m sec^{-1} (assuming $h_o = 10^7$m - the depth of penetration of the flow), or a phase velocity at the feet of:

$$c = 6 \times 10^9 k_f \quad m\ sec^{-1} \tag{30}$$

where k is the wave number. Inspection of Fig. 1 shows that the dominant wavelength is of the order 10^6m. Thus $c \sim 4 \times 10^4$m sec^{-1}. This is a factor of 40 faster than the observed velocity of the westward surge, which must, therefore, violate the assumptions if it is a surface wave on the closed section of the magnetosphere.

c. The bulge shape

The shape of the bulge to the east is similar to that expected from the diffusion equation, but the westward travelling surge is quite different from that predicted by equation (29). A numerical treatment of the non-linear equation (28) gives the same order of magnitutde for the velocities, and the wave shape is similar to that observed in heat flow problems. Thus the shape of the westward travelling surge cannot be accounted for by equation (28).

The basic east-west asymmetry is probably a result of the earth's rotation. The velocity of the feet due to rotation is $\approx$ 130 m sec^{-1}, whereas the observed drift velocities are $\approx$ 300 m sec^{-1}. Thus at any given time, auroral patches and irregularities to the east, in Fig. 1, are two or three times further away from the midnight meridian than those to the west.

An asymmetry in the shape of the bulge is expected

if it is assumed that the recombination slot remains fixed in local time, while the earth and closed region rotate under it. Fig. 13 shows the expected shape of the bulge after 1/2 hr, allowing for addition on an area six earth radii wide, and allowing east-west spread at the rate of 10 km sec^{-1} (the map of 300 m sec^{-1}) from the time of deposition of a particular layer of the bulge.

d. The westward travelling surge

Although the existence of an east-west asymmetry can be explained as above, it still offers no explanation of the steep front of the westward travelling surge. Several possibilities are discussed here which might, by themselves, or in combination cause such a shape:

(1) It has been assumed thus far that the recombination slot has a width of about 6 earth radii. If this width increased as the substorm progressed, the surge would be the map of the edge of the slot, the northward motion of the auroral arcs being of the same nature as the northward motion near midnight, i.e. the mapping of the outward motion of the inner edge of the neutral sheet.

(2) The field lines in the tail can flow in from the sides, as well as the top, to replace the annihilated field in the tail (see Fig. 14). These field lines can then recombine through the slot, be added to the bulge, and return to their

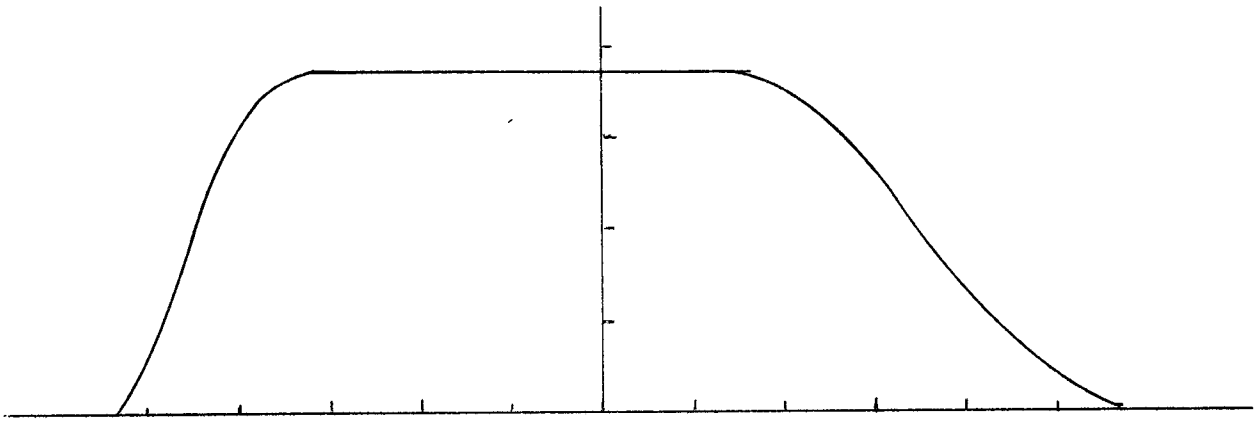

Fig. 13. Asymmetry of the bulge. It is assumed that recombined field lines are added through a slot 6 earth radii wide, for 1/2 hr while the earth rotates under the slot. Each layer is assumed to spread at 10 km sec^{-1} from the time of its deposition.

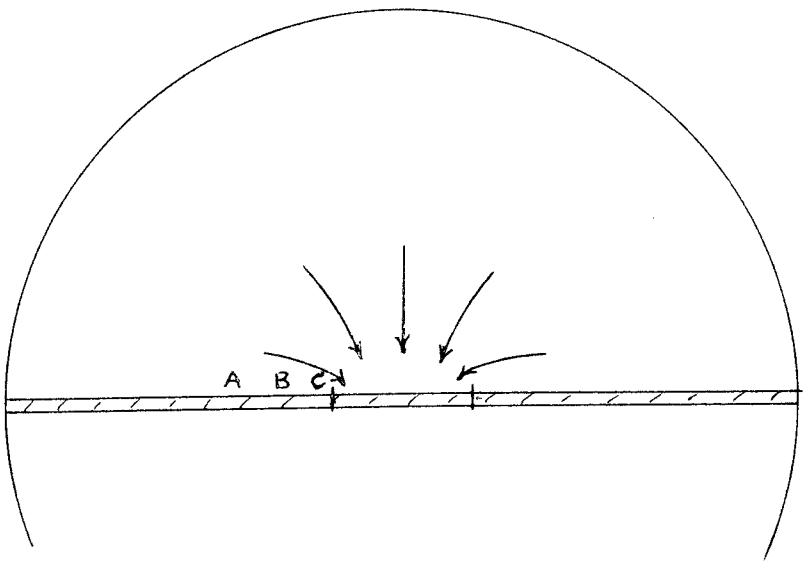

Fig. 14. Flow in the tail into the region of annihilation. This is a cross section of the tail.

original longitude with little or no motion of their feet, i.e. the flow takes place by distortion of the field lines. As seen at the earth, this would be similar in appearance to (1) above, and would account for the features of the westward surge.

(3) The feet of the outer field lines are at higher latitudes. This effect was ignored due to the Cartesian coordinate system approximation. If a field line in the top of the surge (co-latitude 16° - see fig. 1 d) is compared with one at the base (colatitude 21°), the ratio of energy losses ($\underset{\sim}{F} \cdot \underset{\sim}{v}$) for the same angular velocity is the ratio of their v_f squared, or $(16/21)^2 = .58$. Thus the top of the bulge should travel faster than is indicated by equation (28), leading to a steeper wave front, and a possible explanation of the westward surge.

(4) In addition to the above flow patterns, a number of magnetic field distortions occurring in the flow could change the basic wave shape from that predicted by equation (28). For instance, if flux tubes A, B and C in Fig. 14, lying east-west in the tail, and anchored east-west in the polar cap, are deposited on top of each other in the bulge, as might be expected from the flow, then there is a twist in the flux tube which will result in torsion along a flux tube. With this, and other types of distortion that could occur, it is quite possible that the shape of the flux tube

that makes up the bulge is quite different at the equator and at the feet.

In Figs. 1 c and d there is a high latitude auroral arc which moves northward just ahead of the westward surge. This is consistent with the idea of a spreading bulge, as there must be northward movement of the tail field lines' feet in order to accommodate the bulge. This favours (3) and (4) above, as does the existence of westward drift. However, (1) and (2) cannot be discounted entirely on these grounds, as the resultant flow still depends on whether h in equation (24) is greater at the midnight meridian or at the surge.

As the bulge continues to spread in the recovery phase, there is a general southward motion of the northern edge of the auroral arcs (Figs. 1 e and f), as must be expected if the bulge spreads without further addition of fluid. This motion does of course involve foot dragging, and is consequently slower than the original northward expansion.

e. EGO satellite observations

Now consider Fig. 4, the results of Heppner, 1965. EGO satellite observed sudden decreases in field strength at 1937 and 2139 U.T. Two possible explanations of this are offered:

(1) 10^8 webers of tail field are annihilated, causing a decrease in the tail field strength. There are two objections to this. The approximate time for an expansion wave to cross the tail is about 5 min, so that it is rather difficult to account for the bay commencement, observed at the earth, occurring 15 min before the observed decrease at the satellite. The second objection is one of magnitude. The area of field annihilated is about 1.6×10^{15} m^2 in accordance with the model. The area of the upper half tail is 1.5×10^{16} m^2 (15 earth radii radius). Thus the expected decrease is 10% or 4γ, whereas the observed decrease is 40% or 15γ. For these reasons the author prefers the explanation given below.

(2) This involves the westward surge. The satellite local time at these events is 2130. The westward travelling surge can be seen to pass this meridian in Fig. 1 d sometime in the period 10 to 30 min after the substorm commencement, accounting for the 15 min observed delay at the satellite. The amplitude of the surge is 500 km, corresponding to a bulge of about 2 1/2 earth radii. Thus, on the nightside, the boundary of the closed region, and the cusp, or region of depressed magnetic field, may be expected to move outward by about this amount as the surge passes. As the satellite was at low latitudes, and at geocentric distances 10 and

13 earth radii, this movement should place the satellite further in the cusp. The field strength in the cusp varies from zero to the tail field strength, and the decrease could be quite large.

CHAPTER VIII

MAGNETIC EFFECTS

a. Pedersen conductivity

As was discussed in Chapter II, and illustrated in Fig. 7, steady state convection is accompanied by a Pedersen current in the ionosphere which completes its circuit by flowing up the field lines, and then across them, in essence forming a current loop. In any steady-state flow, the feet of the field lines must trace out closed loops in the ionosphere. Consider in particular a plasma convection in a circular pattern over an ionosphere of uniform conductivity. Assume for simplicity that the field lines are vertical. The result is a series of current loops whose normals form circles coaxial with the convection, and the current flow is similar to that in a toroidal coil. A toroidal coil produces little or no exterior magnetic field. Thus such a flow should produce little magnetic effect at the earth's surface. Mathematically it can be stated:

$$\oint \underset{\sim}{B} \cdot d\underset{\sim}{\ell} = \mu_0 \iint \underset{\sim}{J} \cdot d\underset{\sim}{A} \tag{31}$$

The line integral is taken along a circle on the earth's surface directly underneath and coaxial with the convecting

flow (see Fig. 15). J through such a circle is zero, and symmetry requires that B be the same everywhere i.e. zero since the R.H.S. of equation (31) is zero.

Consider the case where the convecting slab is not of uniform thickness. The horizontal field component just above the ionosphere due to the Pedersen current loops is

$$B_h = \mu_0 J = \mu_0 \sigma_\perp v_f B_f$$

and hence

$$B_h w = \mu_0 \sigma_\perp v_f B_f w \tag{32}$$

where w is the thickness of the slab. For a steady-state flow, $v_f B_f w$ is a constant at any cross section, and thus the total horizontal magnetic flux remains constant within a convecting slab, implying that the field lines due to the Pedersen current tend to stay inside the slab, except perhaps at places where there are sharp changes in geometry. Thus one can say that in general, a steady-state Pedersen current produced by convection produces magnetic effects much smaller than those predicted by the sheet current approximation if the Pedersen conductivity of the ionosphere is reasonably uniform.

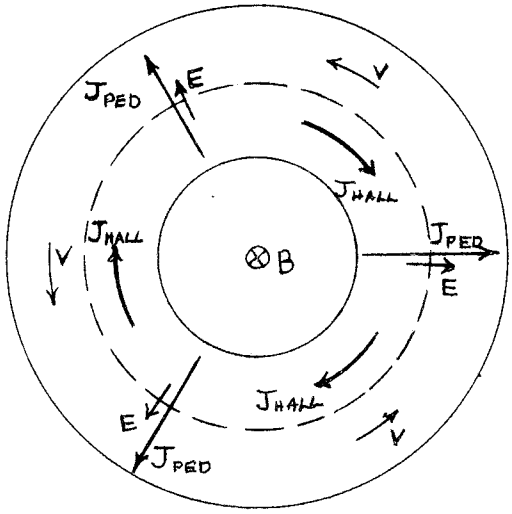

Fig. 15. Symmetry of the Pedersen current system. The line integral is taken along the dotted line, which is below the ionosphere.

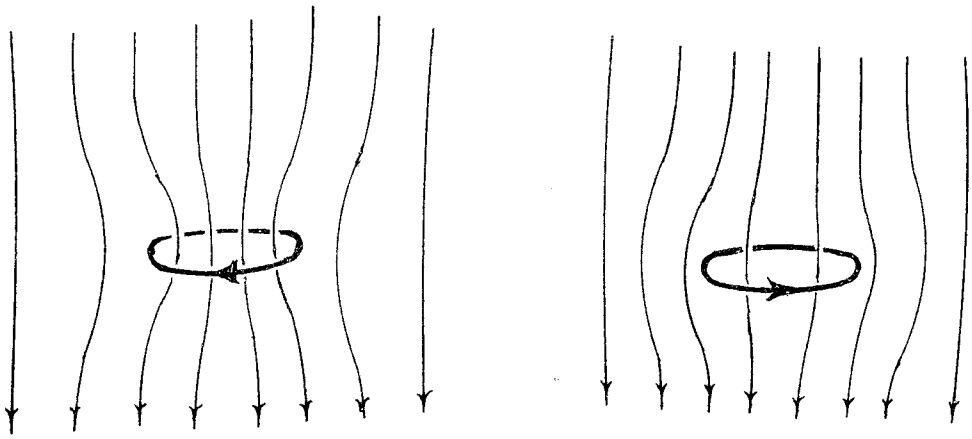

Fig. 16. Effect of Hall currents on the magnetic field lines.

b. Hall conductivity

The Hall conductivity exists because the electrons stay frozen to lower levels than do the protons, and can consequently follow the motion of the flux tube feet at lower levels. Electron motion in the direction of flux tube flow is a current in the opposite direction. The result in a closed steady-state convection flow is that the feet of field lines are crowded together, or diminished inside the Hall current loops, as shown in Fig. 16.

c. Current systems in the ionosphere

Most estimates of ionospheric conductivities yield values for the ratio of the height integrated Pedersen conductivity to the height integrated Hall conductivity in the range from 1:10 to 1:1. However, the considerations at the beginning of this chapter show that the Pedersen conductivity should have little magnetic effect at the earth's surface, so that much of the observed effect is probably due to Hall currents. These occur at an altitude of about 100 km. As the spatial variation on the earth's surface usually involves distances greater than this, the sheet current approximation should be reasonable. ($B = \mu_0 J/2$) Thus the flow pattern of flux tube feet in the ionosphere may be expected to produce the same pattern for the currents, but with the direction reversed. Fig. 17

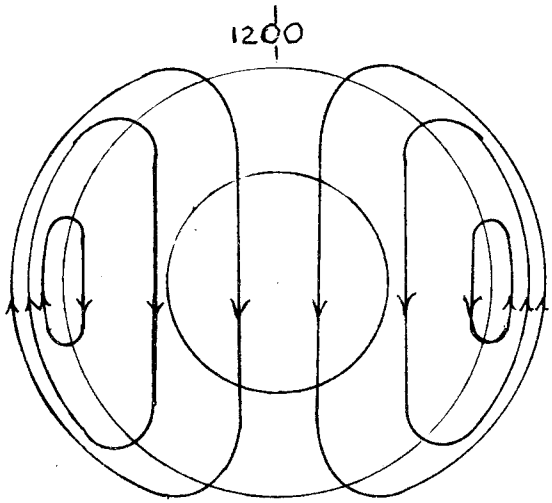

Fig. 17. Flow of flux tube feet for a nonrotating earth. Reverse the flow directions to get the current system.

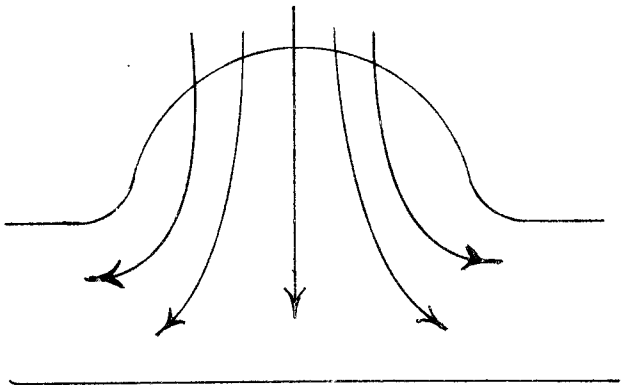

Fig. 18. Flow of flux tubes into the bulge.

shows the type of steady-state flow which might be expected for a non-rotating earth, with steady-state convection and interchange occurring as described in earlier chapters. The current pattern produced by this has some features in common with those in Fig. 3. The rotation of the earth, and the non steady-state that exists in a substorm would be expected to modify this pattern somewhat. However, it seems unlikely that it is capable of accounting for the strong westward electrojet that is observed on the nightside.

Consider the cross polar cap flow produced by a polar substorm. For field lines in the tail, motion is controlled by hydromagnetic wave velocities. However, the motion of their feet is controlled by the foot dragging effect of the ionosphere, and may thus be expected to be slower. The annihilation of field results in flow toward the neutral sheet at 1/10 of the Alfven velocity. The corresponding motion of flux tube feet across the polar cap towards the nightside will lag this. Thus the feet flow across the polar cap during a bay, should equal the flux annihilated at the neutral sheet during the implosion. The duration of a bay is 4000 sec, and the corresponding potential across the polar cap is 10^8 webers/4000 sec = 2.5×10^4 volts. This is of the correct order of magnitude for fields calculated from the bay current system (e.g. Taylor and Hones, 1965). Thus the Hall current can account for the cross polar cap flow.

d. Westward electrojet

It has been indicated (Kim and Kim, 1963) that the height integrated conductivities in an aurora excited ionosphere might be as much as two orders of magnitude greater than that in a quiet ionosphere. Thus, a high conductivity strip might be expected all along the auroral arcs. The addition of fluid into the bulge, and the return flow toward the dayside means that there is a southward flow of flux tube feet across the auroral arcs, as shown in Fig. 18. This flow should cause a large Pedersen current in the high conductivity strip, which being long and thin, gives a current similar to a single loop, rather than the toroidal current system discussed earlier. The previous paragraph predicted a cross polar cap voltage of 2.5×10^4 volt, or an electric field of 0.006 v m^{-1}. For a height integrated Pedersen conductivity of 2×10^2 mho in the high conductivity strip (Kim and Kim, 1963) the height integrated Pedersen current is 1.2 amp m^{-1}. Using the sheet current approximation, this gives a magnetic field of 600γ, and thus gives an adequate explanation of the westward electrojet.

CHAPTER IX

DISCUSSION

The model of the magnetosphere as presented herein contains many features of earlier models, including those of Axford and Hines (1961), Axford, Petschek and Siscoe (1965), Dungey (1963), Ness (1965). The new features of the present model are:

(1) Recombination occurs impulsively at the neutral sheet causing polar substorms.

(2) Recombination is limited to a width of 6 or 7 earth radii in the tail.

(3) The "foot dragging" effect is found to dominate the inertial and viscous effects in the flow of flux tubes. This is taken into account in the development of the model.

(4) A large bulge is formed on the nightside, driving the return flow, and probably creating a wave-like feature on the nightside of the closed region.

(5) The effect of the Pedersen current is negligible at the surface of the earth, except for the conductivity anomaly along the auroral arcs, where it could be the cause of the westward electrojet.

During the last few months of the preparation of this thesis, the author has received preprints from W. I. Axford and J. W. Dungey, both of whom have advanced what is essentially the same model, i.e. substorms are the results of impulsive recombination in the geomagnetic tail. However, the development in the three cases is quite different.

There are a few other experimental observations which might be explained in terms of the model:

(1) As the Anderson (1965) electron islands start at the outside of the cusp region, and their energies are similar to those causing auroral X-rays, it is possible that they are the other half of the recombination process proceeding outwards along the tail. It would be interesting to look for a correspondence with substorms.

(2) The observation of Carpenter (1966) of a sudden increase in the equatorial radius of the electron knee around 1800 LMT could be explained in terms of a type of stagnation point, as Carpenter suggested. This would be an average stagnation point as the fluid added by successive substorms tried to flow upstream around the evening side. Its size and position would depend on the substorm size and occurrence frequency. Carpenter observed that the knee becomes more symmetric with decreasing geomagnetic activity, and that the position of the increase in radius varies over several hours in local time. It would be interesting to look for

a correspondence between knee position and size, and westward surge events, or substorm frequency.

Many features of the model can be tested by satellite results. It is desirable to see what is happening at many positions on the nightside during substorms, both to the magnetic field, and to the particles. In particular, more observations in the range 7 to 14 earth radii, between 1800 and 0600 LMT, and their comparison with polar substorm events are needed.

BIBLIOGRAPHY

Akasofu, S.-I., The development of the auroral substorm, Planet. Space Sci., 12, 273, 1964.

Akasofu, S.-I., S. Chapman and C.I. Meng, J. Atmos. Terr. Phys., 24, in press, 1965.

Anderson, K.A., Energetic electron fluxes in the tail of the geomagnetic field, J. Geophys. Res. 70, 4741, 1965.

Axford, W. I., Viscous interaction between the solar wind and the earth's magnetosphere, Planet. Space Sci. 12, 45, 1964.

Axford, W.I., C. O. Hines, A unifying theory of high latitude geophysical phenomena and geomagnetic storms, Can. J. Phys., 39, 1433, 1961.

Axford, W.I., H.E. Petschek, G. L. Siscoe, Tail of the magnetosphere, J. Geophys. Res. 70, 1231, 1965.

Carpenter, D. L., Whistler studies of the plasma-pause in the magnetosphere, J. Geophys. Res. 71, 693, 1966.

Chamberlain, J. W., Physics of the aurora and airglow, Academic Press, New York, 1961.

Davis, L. R., Enhancement of trapped protons during the magnetic storm of April 18, 1965, Am. Geophys. Union, 47th Annual Meeting, Washington. Paper 57a. 1966.

Dungey, J. W., Cosmic electrodynamics, Cambridge Univ. Press, 1958.

Dungey, J. W., Structure of the exosphere or adventures in velocity space, Geophysics The Earth's Environment, Gordon and Breach, New York, 1963.

Fukushima, N., Polar magnetic storms and geomagnetic bays, J. Fac. Sci. Tokyo Univ. 8, 293, 1953.

Gold, T., Motions in the magnetosphere of the earth. J. Geophys. Res. 64, 1219, 1959.

Heppner, J. P., Recent measurements of the magnetic field in the outer magnetosphere and boundary regions, NASA X-612-65-490.

Kim, H. Y., J. S. Kim, Atmospheric conductivities over Fort Churchill, J. Atmos. Terr. Phys., 25, 481, 1963.

Ness, N. F., The Earth's magnetic tail, J. Geophys. Res. 70, 2989, 1965.

Ness, N. F., C. S. Scearce, J. B. Seek, J. M. Wilcox, A summary of results from the IMP-1 Magnetic field experiment, NASA X-612-65-180, 1965.

O'Brien, B. J., H. Taylor, High-latitude geophysical studies with Satellite Injun 3. 4. Auroras and their excitation, J. Geophys. Res. 69, 45, 1964.

Parker, E. N., Interplanetary dynamical processes, Interscience, New York, 1963.

Parker, E. N., Interaction of the solar wind with the geomagnetic field, Phys. Fluids, 1, 171, 1958.

Petschek, H.E., Magnetic field annihilation, AAS-NASA Symposium on the physics of Solar Flares, ed. by W. N. Hess, NASA SP-50, 1964.

Piddington, J. H., Geomagnetic storm theory, J. Geophys. Res. 65, 93, 1960.

Piddington, J. H., Geomagnetic storms, auroras and associated effects, Space Sci. Rev. 3, 724, 1964.

Spreiter, J. R., A. L. Summers, A. Y. Alksne, Hydromagnetic flow around the magnetosphere, Planet. Space Sci. 14, 223, 1966.

Sweet, P.A., The neutral point theory of solar flares, I.A.U. Symposium No. 6., ed. by B. Lehrest, Cambridge Univ. Press, 1958.

Taylor, H. E., E. W. Hones, Jr., Adiabatic motion of auroral particles in a model of the electric and magnetic fields surrounding the earth, J. Geophys. Res. 70, 3605, 1965.

APPENDIX I

Symbols and Conventions Used

A	Cross sectional area of flux tube. Also: constant in (19b)
B	Magnetic field
B_h	Horizontal component of magnetic field
c	Phase velocity
d	Distance scale perpendicular to the magnetic field
E	Electric field. Also: Energy of particles
f	As a subscript denotes the value at the feet of the field lines
F	Force
g	Mapping factor along a flux tube, feet to equator
h	Height as defined by Fig. 12
j	Current in the magnetosphere
J	Current
J_i	Pedersen current in the ionosphere
l	Length scale of field lines. Also: Coordinate along field lines.

n	Number density of particles
p	Gas pressure
P	Magnetohydrodynamic pressure ($P = p + B^2/2\mu_0$)
r	Coordinate
r_o	Radius of the earth
r_e	Radius of a field line in the equatorial plane
R	Radius of curvature of a field line.
s	Arc length
T, t	Time
v	Velocity of fluid element
V	Volume
V_A	Alfven velocity in the tail
W	Thickness of the slab
x	Coordinate
y	Coordinate
z	Coordinate
α	Latitude

α_0	Latitude of the feet of a field line
γ	Unit of magnetic field (10^{-5} gauss)
θ	Angular coordinate (longitude)
λ	A Lamé constant
μ	Dynamic viscosity (Lamé constant)
ν	Kinematic viscosity
ρ	Mass density
$\sigma_\perp$	Height integrated Pedersen conductivity
τ	Maxwell stress tensor

APPENDIX II

Mapping Factors in a Dipole Field

Throughout the thesis it has been assumed that $g_\theta = g_r = g$, whereas in actual fact $g = \sqrt{g_r\, g_\theta}$. However, the approximation is sufficiently accurate provided that $g_r / g_\theta \approx 1$. The mapping factors for a dipole field are considered and it is shown that this is true for a reasonable field configuration. The geometry is shown in Fig. 19.

In the angular direction:

$$\frac{ds_1}{ds_2} = \frac{r_e}{r_0}$$

$$\frac{ds_3}{ds_2} = \cos\alpha_0$$

$$\therefore \quad \frac{ds_1}{ds_3} = \frac{r_e}{r_0 \cos\alpha_0}$$

For a field line:

$$r = r_e \cos^2\alpha$$

$$r_0 = r_e \cos^2\alpha_0$$

$$\therefore \quad \frac{ds_1}{ds_3} = g_\theta = \frac{1}{\cos^3\alpha_0} \tag{33}$$

In the radial direction:

$$r_0 = r_e \cos^2\alpha_0$$

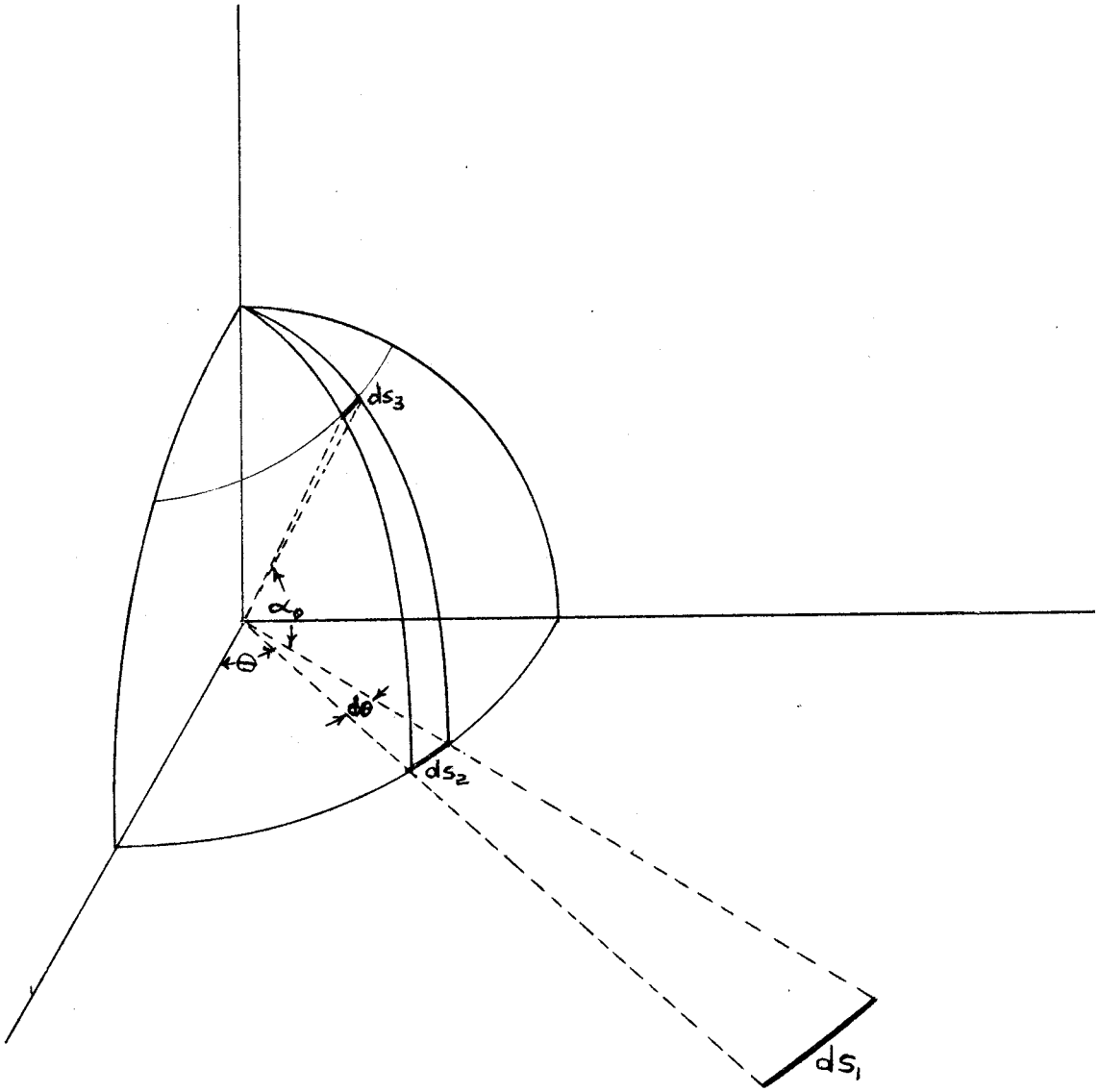

Fig. 19. Mapping factors for a dipole field.

Differentiation gives

$$\frac{d\alpha_0}{dr_e} = -\frac{\cos\alpha_0}{2r_e\sin\alpha_0}$$

Hence

$$g_r = \left|\frac{r_0\, d\alpha_0}{dr_e}\right|^{-1}$$

$$= \frac{2r_e\sin\alpha_0}{r_0\cos\alpha_0}$$

$$= \frac{2\sin\alpha_0}{\cos^3\alpha_0} \qquad (34)$$

From equations (33) and (34),

$$g_r = 2\sin\alpha_0\, g_\theta$$

The theory involves field lines for which $60° < \alpha_0 < 90°$. Thus $2\sin\alpha_0$ and hence $\frac{g_r}{g_\theta}$ varies between 1 and 2 in the region of interest for a dipole field.